DESIGN OF METAMATERIAL BASED PATCH ANTENNA

A PROJECT THESIS

By

Farisha T (EE12M005)

Submitted in partial fulfilment of the requirements for the award

of the degree

MASTER OF TECHNOLOGY

Under the guidance of

Dr. V. Subramanian

&

Dr. Sarathi . R

DEPARTMENT OF ELECTRICAL ENGINEERING

INDIAN INSTITUTE OF TECHNOLOGY MADRAS

CHENNAI – 600036

MAY 2014

CERTIFICATE

This is to certify that the thesis entitled **"DESIGN OF METAMATERIAL BASED PATCH ANTENNA"** submitted by **Farisha T** to Indian Institute of Technology Madras, Chennai for the award of degree of **Master of Technology in Communication Systems,** is a bonafide record of project work carried out by her under my supervision and guidance. The contents of this thesis, in full or in parts, have not been submitted to any other Institute or University for the award of any degree or diploma.

Project Guides

1. **Prof.V. Subramanian**

   Microwave Laboratory

   Department of Physics

   Indian Institute of Technology Madras

2. **Prof. Sarathi. R**

   High Voltage Laboratory

   Department of Electrical Engineering

   Indian Institute of Technology Madras

Chennai: 600036

Date :

ACKNOWLEDGEMENT

First and foremost, I am deeply indebted to my project guides **Dr. V. Subramanian** and **Dr. R. Sarathi** for their guidance and encouragement throughout the course of this project. I would like to thank them profusely for their patient guidance even at difficult times.

I would also like to thank **Dr. Krishna S**, M.Tech. Project Coordinator, Electrical Engineering Department, for his help and support for the final completion of my work.

It is a pleasure to thank all my labmates, especially **Rajkumar R**, **Liny Stephen** and **S. Dinesh Kumar**, without whom some of my work would not have been possible. I am really thankful to all of them.

I am highly thankful to **Dr. N. Yogesh**, currently doing Post Doctorate at Shenzhen University, China for his valuable support during initial stages of my work.

Finally, since a mere word of thanks would be really insufficient to express my gratitude to my parents and other family members, I would like to dedicate my work to them.

FARISHA T

ABSTRACT

Electromagnetic metamaterials are artificial effectively homogeneous structures that can be designed to exhibit specific electromagnetic properties not commonly found in nature. The prefix "meta" means "beyond" in Greek. These structures are regarded as metamaterials because they are beyond our experience and the descriptions we give to normal bulk materials. These structures have average cell size less than the guided wavelength and can result in effective medium parameters unattainable in natural materials. An interesting feature is that they can attain negative permeability and permittivity. A metamaterial with negative permeability and permittivity is known as Left Handed Metamaterial (LHM).

In recent years, these structures are widely applied in antennas for fixed and mobile communications system because of their interesting features when interacting with electromagnetic waves.

In this project, a planar zero-index metamaterial is designed. The simulation results show that a zero index of refraction occurs at 10.255 GHz. The zero index of refraction can be used to enhance the directivity of antennas. A microstrip patch antenna designed at the same above frequency, showed an improvement in directivity with the help of a zero-index metamaterial as superstrate. The above antenna is fabricated and experimentally verified.

The thesis also highlights the design of a metamaterial for steering the beam of a microstrip patch antenna. The varying refractive index of the metamaterial helps to achieve the steering of the beam of the antenna.

TABLE OF CONTENTS

LIST OF FIGURES

LIST OF TABLES

ABBREVIATION AND SYMBOLS

e-m	Electromagnetics
LH	Left - Handed
RH	Right - Handed
PEC	Perfect Electric Conductor
S21	Transmission coefficient
S11	Reflection coefficient
ZIM	Zero-index medium

Greek Symbols

ε_r	Relative dielectric permittivity
ε_r' `	Real part of complex dielectric permittivity
ε_r''	Imaginary part of complex dielectric permittivity
μ_0	Permeability of free space
μ_r	Relative magnetic permeability
ω	Angular Frequency
θ	Elevation angle
ϕ	Azimuth angle
n	Refractive index

CHAPTER 1

INTRODUCTION

1.1 METAMATERIALS

Metamaterials are engineered media whose electromagnetic responses are different from those of their constituent components. There are several classifications of metamaterials. They are named based on their fundamental properties, i.e., by the signs of their permittivity and permeability. The double positive (DPS) metamaterials have both the permittivity and permeability positive, i.e., $\varepsilon > 0$, $\mu > 0$. The double negative (DNG) metamaterials have both the permittivity and permeability negative, i.e., $\varepsilon < 0$, $\mu < 0$. The single-negative (SNG) metamaterials have either the permittivity or the permeability less than zero. The epsilon negative (ENG) metamaterials have the permittivity less than zero, i.e., $\varepsilon < 0$, $\mu > 0$. The mu negative (MNG) metamaterials have the permeability less than zero, i.e., $\varepsilon > 0$ $\mu < 0$.

Left-Handed Materials (LHM) were first theorized by Veselago [1] as double negative materials (DNG) for their simultaneously negative permittivity (ε_r) and permeability (μ_r). The term "left-handed" describes the fact that the vectors **E** (electric field), **H** (magnetic field) and **k** (wave vector) form a left-handed triplet, instead of a right-handed triplet, as is the case in conventional right-handed (RH) media. Although Veselago's prediction was brought out in 1967, experimental verifications of the effective permeability and the left-handedness were presented by Pendry and Smith [2] three decades later. Thus, in LH media, the Poynting vector **S** (that points at the direction of energy propagation and the group velocity) is anti-parallel to the wave vector **k** (that points at the direction of phase velocity).

These LH materials possess a negative effective refractive index n (NRI) related to the phase velocity according to $V_p = \frac{\omega}{\beta} = \frac{c}{n}$, where c is the velocity of light in free space. For NRI metamaterials, phase velocity ($V_P = \omega/ß$) and the group velocity, $V_g = \frac{\delta\omega}{\delta\beta}$ are anti-parallel.

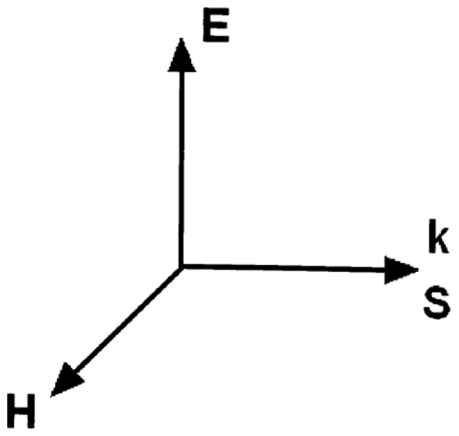

1.1a)

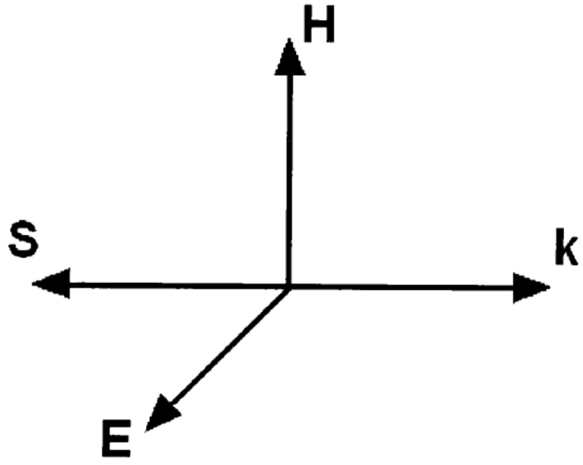

1.1b)

Figure1.1: a) Right handed medium b) Left handed medium

1.2 APPLICATION IN ANTENNA DESIGN

With the development of metamaterial studies, some research works concluded that when the ray is incident from inside the zero-index medium (ZIM) into the free space, the refracted rays will be normal to the interface. This special property provides a unique method of controlling the direction of emission. In 2002, Enoch [3] experimentally demonstrated for the first time that energy radiated by a source embedded in a metallic grids structure will be concentrated in a narrow cone in the surrounding media when the

refractive index of metamaterials is close to zero in some frequency bands, so a great improvement of directivity was potentially obtained. This material can be used to improve the directivity of antennas.

An array of continuous thin wires are characterized by a plasma frequency [4, 5], $\varepsilon_{eff} = 1 - \frac{\omega_p{}^2}{\omega^2}$, where ω_p is the plasma frequency and ω is the frequency of the propagating electromagnetic wave. The refractive index $n = \sqrt{\varepsilon_{eff}\,\mu_{eff}}$ approaches zero, on the condition that the operating frequency is very close to the plasma frequency, where μ_{eff} is the effective permeability. According to the Snell's law, when the ray is incident from inside the low-index metamaterial or zero-index metamaterial into free space, the angle of refraction will be close to zero, and the refracted rays will be normal to the interface. This property provides a unique method of designing high-directive antennas.

The advance of the wireless telecommunications networks ought to develop smart antenna systems. For a best quality of service, it is necessary to dynamically steer the radiation of the antennas in privileged directions and to present nulls in all the other directions for interference minimization. For this purpose, phased arrays are a well proven technology; however it does not really fit in mobile terminals due to limited space availability. This thesis proposes the covering of a primary radiating source by a metamaterial superstrate based on an omega shaped unit cell having a varying index medium, in order to introduce the beam steering control of the antenna. The tuning of the metamaterial resonators is obtained by varying the gap impedance of the omega cell by an appropriate loading through a varactor diode or by using variable capacitor.

1.3 OBJECTIVE

In this thesis, the objective is to design a zero index metamaterial at a frequency of 10.255 GHz and to realize a directive patch antenna using this ZIM.

The thesis also proposes an omega (Ω) shaped metamaterial for steering the beam of the microstrip patch antenna.

1.4 ORGANIZATION OF THE THESIS

This chapter present the introduction, problem definition, antenna design application and objective of this thesis work.
Chapter 2 reports the study of metamaterial parameters. This chapter clearly explains the procedure for parameter retrieval of the metamaterials.

Chapter 3 presents the design of microstrip patch antenna. The scattering parameter and radiation pattern of the antenna is observed. The experimental verification of the design is done and compared with the simulated results.

Chapter 4 explains the design of a zero index metamaterial as a superstrate for microstrip patch antenna. This chapter analyses scattering parameter and the radiation pattern of the antenna. The radiation pattern clearly indicates the improvement of directivity of the antenna. The experimental verification of the design is done for comparison with the simulated results.

Chapter 5 highlights the design of omega (Ω) shaped metamaterial for shifting the beam of the microstrip patch antenna. This chapter shows the steered radiation pattern.

Chapter 6 presents the summary and conclusions.

CHAPTER 2

STUDY OF METAMATERIAL PARAMETERS

2.1 PARAMETER RETRIEVAL

The electromagnetic properties of a structure are determined by well-defined material constants, permittivity (Ɛ), and permeability (μ). Therefore, the extraction of the material constants of a given metamaterial is important for predicting the electromagnetic properties of the metamaterial.

When a Transverse Electromagnetic (TEM) wave is incident on the structure, tangential electric and magnetic fields become zero on PEC and PMC surfaces respectively. Therefore, a fictitious waveguide possessing the PEC surfaces on the top and bottom walls and the PMC surfaces on the front and back walls can support TEM waves. If unit cells of a periodic structure are symmetric, the field distributions in the waveguide for one unit cell are identical with those of the infinite periodic structure. The below Figure 2.1 is taken from [6].

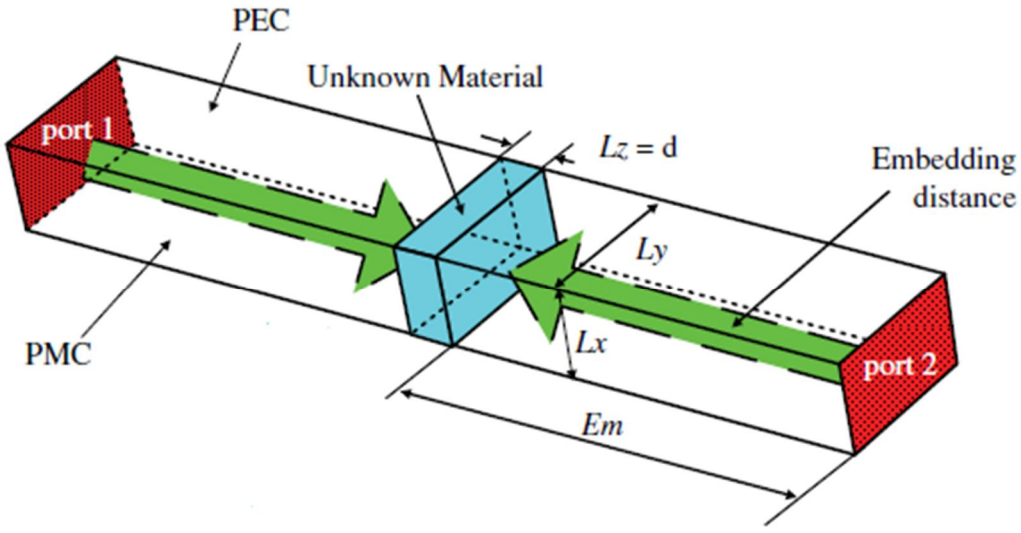

Figure2.1: TEM wave incident on a metamaterial with dimension L_x, L_y and L_z = d

Figure 2.1 shows the waveguide simulation scheme for acquiring *S*-parameters of an unknown material. The PEC boundary condition is applied to the upper and bottom walls at the waveguide, and the PMC boundary condition is applied to the front and back walls.

The length and width of the material with thickness L_z (d) are L_x and L_y, respectively. The scattering parameters at the material's interface are obtained by shifting a phase reference plane from the ports to the material's interfaces (E_m). After the *S*-parameters are obtained, the material constants can be extracted by using the following formulae.

The equation for reflection coefficient and wave impedance are given by

$$\Gamma_{12} = \frac{1-(S_{21}^2 - S_{11}^2)}{2S_{11}} \pm \sqrt{\left[\frac{1-(S_{21}^2 - S_{11}^2)}{2S_{11}}\right]^2 - 1} \text{ and } z = \frac{(S_{11} + S_{21}) - \Gamma_{12}}{1-(S_{11}+S_{21})\Gamma_{12}} \quad \ldots\ldots (2.1)$$

The solution that satisfies the condition $|\Gamma_{12}| \leq 1$ is chosen.

$$\frac{\sqrt{\mu_r}}{\sqrt{\varepsilon_r}} = \frac{1+\ \Gamma_{12}}{1-\ \Gamma_{12}} = X, \quad \sqrt{\mu_r \varepsilon_r} = j\frac{c_0}{dw}[\ \ln|z| + j\arg(z)\ ] = Y \quad \ldots\ldots\ldots\ldots\ldots (2.2)$$

where c_0 is the speed of the wave in free space and d is the thickness of the metamaterial.

$$\text{Now, } \varepsilon_r = \varepsilon_{r,real} - j\,\varepsilon_{r,imag} = \frac{Y}{X} \quad \text{and } \mu_r = \mu_{r,real} - j\,\mu_{r,imag} = X.Y \quad \ldots\ldots\ldots\ldots (2.3)$$

Refractive index of the metamaterial can be calculated as $n = \sqrt{\mu_r \varepsilon_r}$ ……... (2.4)

CHAPTER 3

DESIGN OF MICROSTRIP PATCH ANTENNA

3.1 GENERAL EXPLANATION

Antennas play a very important role in the field of wireless communications. Some of them are Parabolic Reflectors, Patch Antennas, Slot Antennas, and Folded Dipole Antennas. Each type of antenna is good in its own properties and usage. It can be said that antennas are the backbone and almost everything in the wireless communication without which the world could have not reached at this age of technology. Patch antennas play a very significant role in the world of wireless communication systems. They are widely used in aircraft, spacecraft and other application for small size, low cost and light weight.

A microstrip patch antenna [7] is very simple in the construction using a conventional microstrip fabrication technique. The most commonly used microstrip patch antennas are rectangular and circular patch antennas. These patch antennas are used as simple and for the widest and most demanding applications. The below Figure 3.1 is taken from [8].

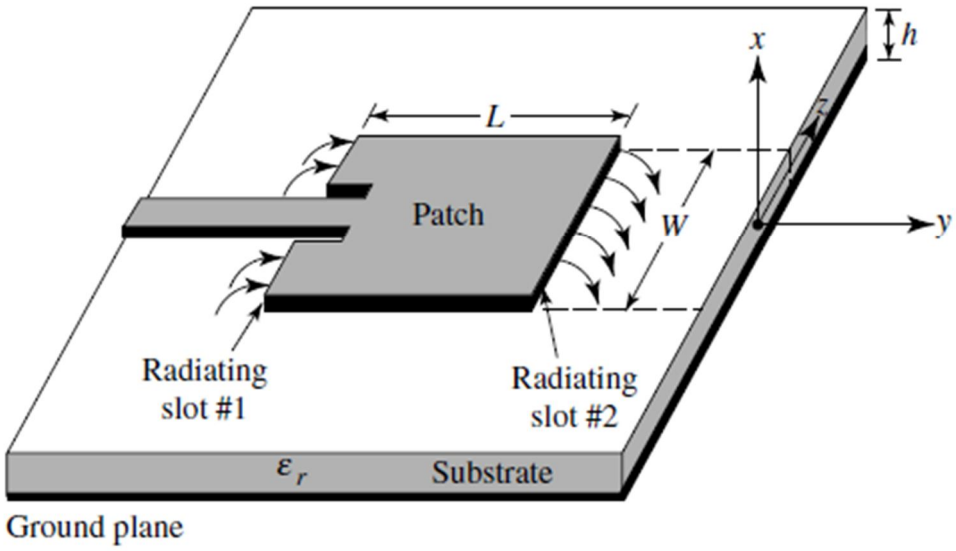

Figure 3.1: Microstrip patch antenna

A microstrip patch antenna is a thin square patch on one side of a dielectric substrate and the other side having a plane to the ground. The simplest microstrip patch antenna

configuration would be the rectangular patch antenna. The patch in the antenna is made of a conducting material, Cu (Copper). A patch antenna has more advantages compared to the other type of antennas due to its cheap cost, portability, installation etc. The integration of these antennas is very easy to other electronic media than the conventional antennas. The basic antenna element is a strip conductor of length (L) and width (W) on a dielectric substrate with constant (ε_r); thickness or height of the patch being (h) with a height and thickness (t) is supported by a ground plane. The rectangular patch antenna is designed so as it can operate at the resonance frequency. The length of the patch for a rectangular patch antenna normally would be $0.333\lambda < L < 0.5\ \lambda$, λ being the free space wavelength. The thickness of the patch is selected to be in such a way that is $t << \lambda$. The height, h, of the dielectric substrate that supports the patch usually ranges between 0.003 λ and 0.05λ so as the dielectric constant, ε_r of the substrate ranging between 2.19 and 12.

Microstrip feed line is used in this project which is one of the simplest form of feeding the patch. Because the dimensions of the patch are finite along the length and width, the fields at the edges of the patch undergo fringing. This is illustrated by the Figure 3.2 which is taken from [8].

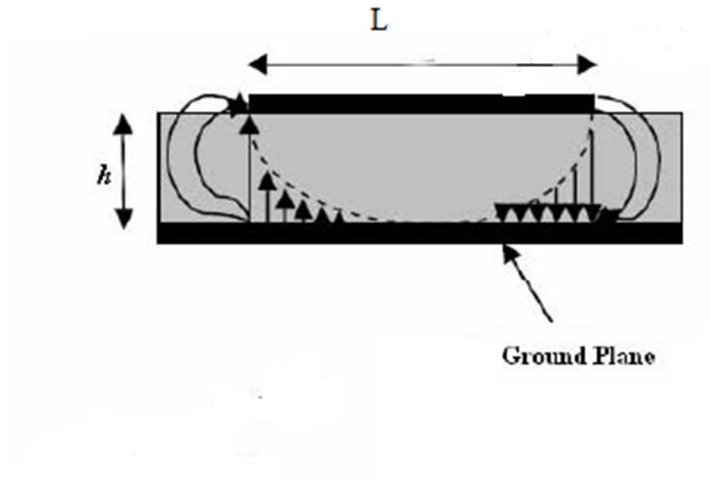

Figure 3.2: Fringing field of microstrip patch

The amount of fringing is a function of the dimensions of the patch and the height of the substrate. Fringing influences the resonant frequency of the antenna. The fringing fields around the antenna can help in explaining why the microstrip antenna radiates. Consider the side view of a patch antenna, shown in Figure 3.2. The current at the end of the patch is zero (open circuit end), the current is maximum at the centre of the half-wave

patch and (theoretically) zero at the beginning of the patch. At the end of the patch the voltage is at a maximum (say +V volts). At the start of the patch antenna (a half-wavelength away), the voltage must be at minimum (-V Volts). Hence, the fields underneath the patch will resemble that of Figure 3.2, which roughly displays the fringing of the fields around the edges. The electric field at the centre is zero and maximum to positive on one side and max to the negative on the opposite side. It is the fringing fields that are responsible for the radiation. The fringing fields near the surface of the patch antenna are both in the +y direction as shown in figure. Hence, the fringing E-fields on the edge of the microstrip antenna add up in phase and produce the radiation of the microstrip antenna. The smaller permittivity or dielectric constant is (ε_r), the more "bowed" the fringing fields become; they extend farther away from the patch. Therefore, using a smaller permittivity for the substrate yields better radiation.

For a microstrip line shown in Figure 3.3, electric field lines reside in the substrate and parts of some lines exist in air. As W/h >> 1 and ε_r > 1, the electric field lines concentrate mostly in the substrate. Fringing in this case makes the microstrip line look wider electrically compared to its physical dimensions. Since some of the waves travel in the substrate and some in air, an effective dielectric constant $\varepsilon_{reff,}$ is introduced to account for fringing.

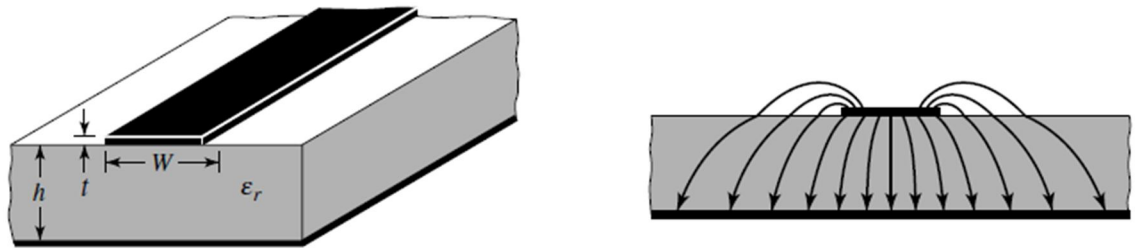

Figure 3.3: Microstrip line and its electric field lines

3.2 PROPOSED STRUCTURE

A patch antenna is designed for a resonant frequency of 10.255 GHz. The structure dimension is as shown below in Figure 3.4. The substrate used was Rogers 5880 with dielectric constant 2.2 and loss tangent 0.0009. The length (L) and width of patch (W) were 9.1 mm and 17.5 mm respectively. Substrate height was about 0.787 mm with metal thickness of about t = 0.035 mm.The substrate size is about 30 mm x 24.895 mm.

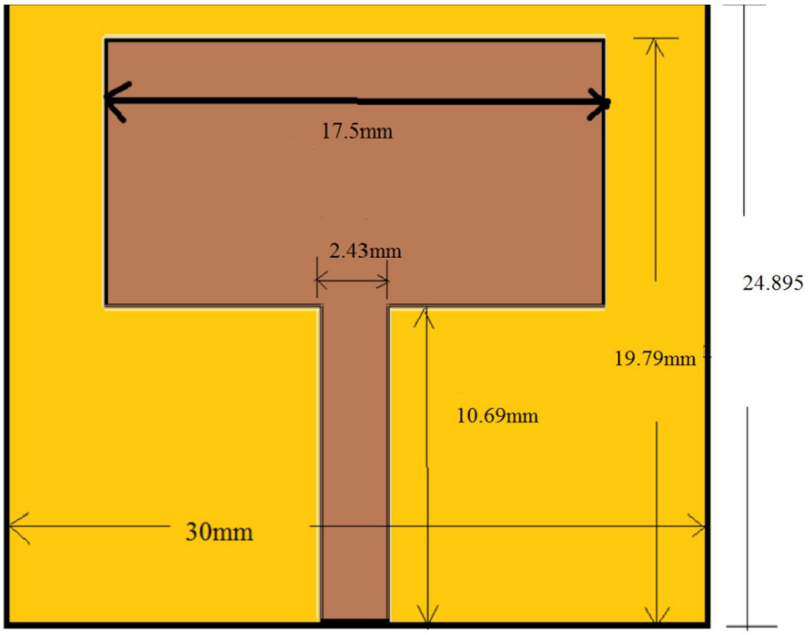

Figure 3.4: Patch antenna corresponding to a resonant frequency of 10.255 GHz.

The figure simulated in CST Microwave Studio is shown in Figure 3.5.

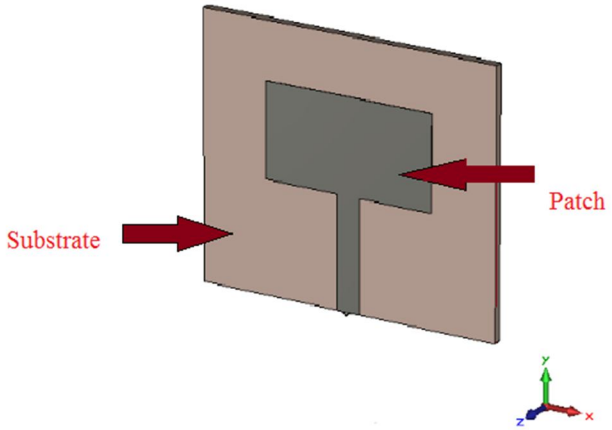

Figure 3.5: Geometry of patch simulated in CST Microwave Studio

3.3 CALCULATION OF DIMENSION

The design equation of the patch is given below.

The width of the patch is, $W = \frac{1}{2f_0\sqrt{\mu_0\varepsilon_0}}\sqrt{\frac{2}{\varepsilon_r+1}}$ ..... (1)

where f_0 is the resonating frequency, ε_r is the permitivity of substrate , μ_0 and ε_0 are permeability and permittivity of free space.

The effective dielectric constant is $\varepsilon_{reff} = \frac{\varepsilon_r+1}{2} + \frac{\varepsilon_r-1}{2}\left[1+12\frac{h}{W}\right]^{\frac{-1}{2}}$ ..... (2)

where h is the height of the substrate. The extended length of patch due to fringing field can be calculated as $\frac{\Delta L}{h} = 0.412\frac{(\varepsilon_{reff}+0.3)\left(\frac{W}{h}+0.264\right)}{(\varepsilon_{reff}-0.258)\left(\frac{W}{h}+0.8\right)}$ ..... (3)

The actual length of patch can be obtained by $L = \frac{1}{2f_r\sqrt{\varepsilon_{reff}\mu_0\varepsilon_0}} - 2\Delta L$..... (4)

3.4 S PARAMETER AND RADIATION PATTERN

The S parameter obtained after simulation in CST microwave is given as

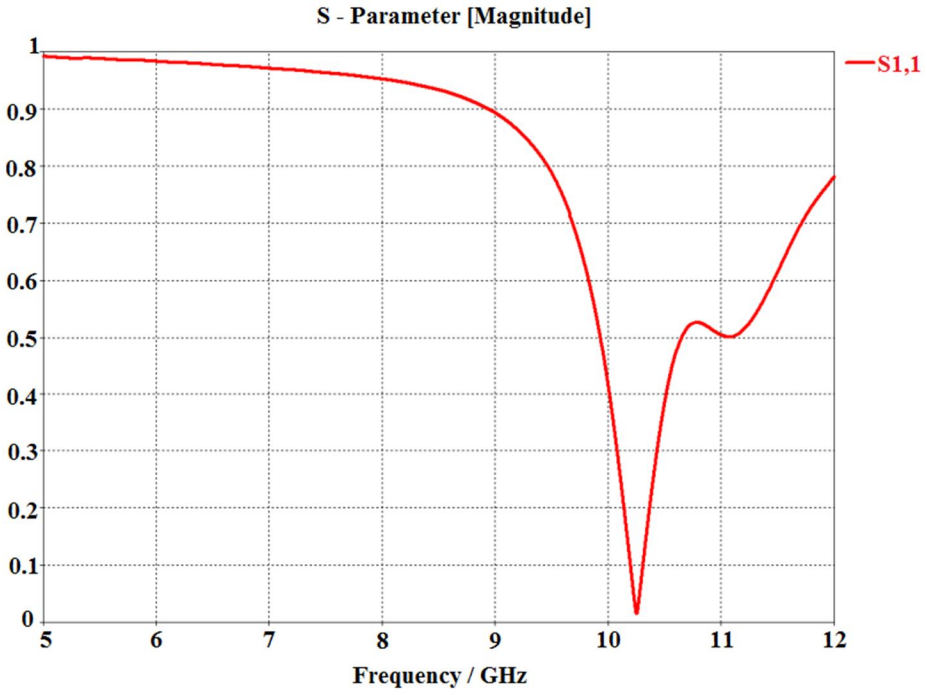

Figure 3.6: S parameter of patch antenna

It can be clearly identified from the figure that the resonating frequency is 10.255 GHz where S11 (reflection coefficient) is about 0.0389.

The radiation pattern diagrams of the patch antenna at the resonant frequency are shown in Figure 3.7 and 3.8.

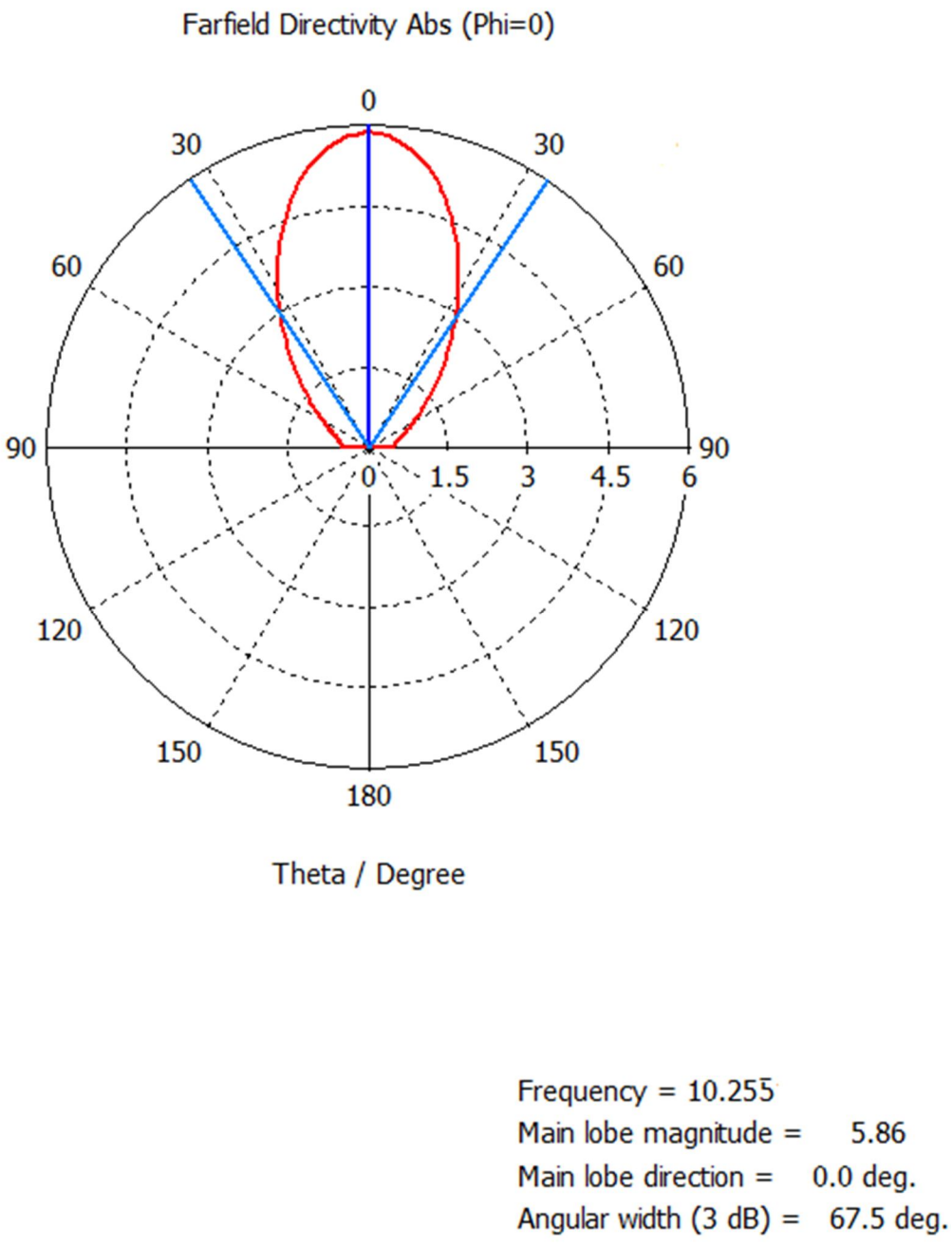

Figure 3.7: Elevation pattern of patch antenna

The above Figure 3.7 shows the elevation pattern of patch antenna with 3dB angular width $\Delta\theta = 67.5^0$. The main lobe magnitude is 5.86 in the linear scale.

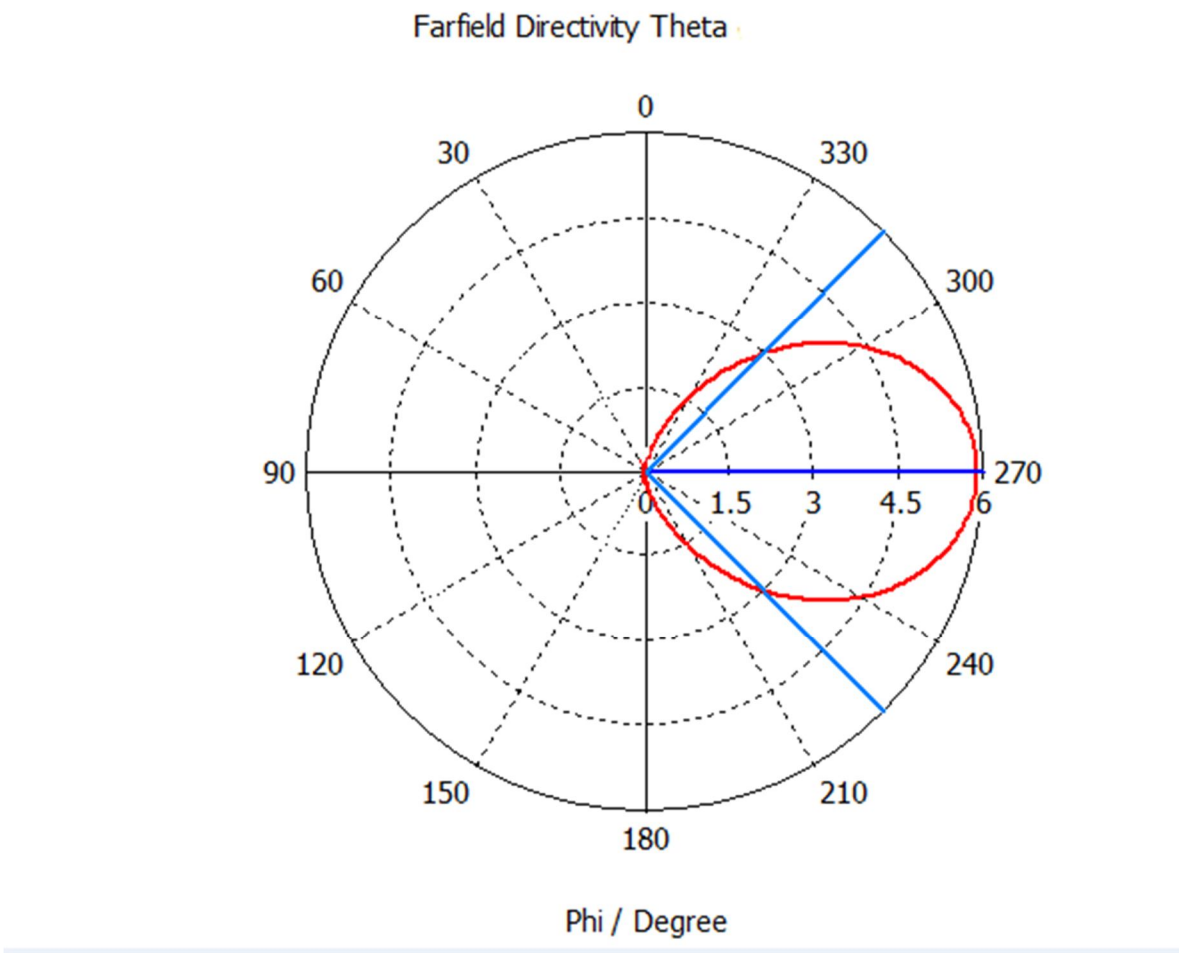

Figure 3.8: Azimuth pattern of patch antenna

The above Figure 3.8 shows the azimuth pattern with 3dB angular width $\Delta\phi = 103.4^0$.

Directivity of the antenna is given by $D = \frac{4\pi}{\Delta\theta\Delta\phi} = 5.87$ (linear scale).

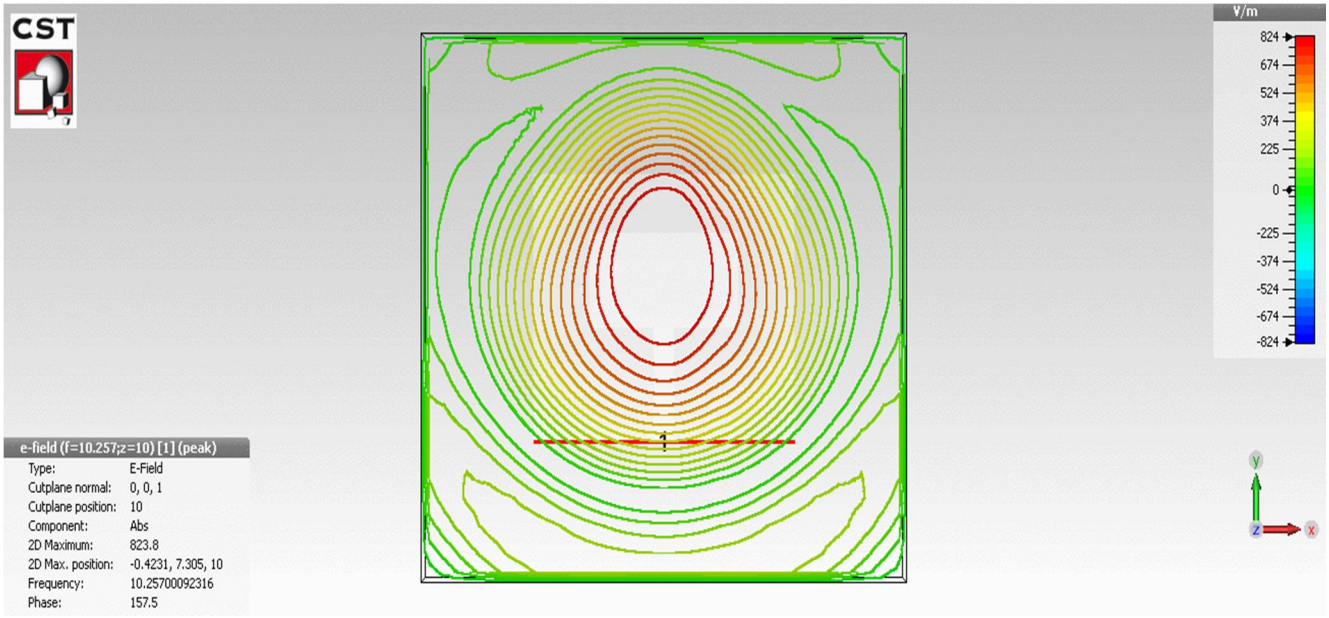

Figure 3.9: Electric field contour plot of patch antenna

The above figure shows the electric field contour plot of patch which indicates spherical wavefronts. This shows that directivity of patch antenna is less.

3.5 EXPERIMENTAL VERIFICATION

The simulated microstrip patch antenna is experimentally verified. It can be seen that experimental results agrees well with simulated results in spite of the fabrication and random errors in the measurement. The fabricated patch antenna is designed for a resonant frequency of 10.255 GHz. The substrate used was Rogers 5880 with dielectric constant 2.2 and loss tangent 0.0009. The length (L) and width of patch (W) were 9.1 mm and 17.5 mm respectively. The substrate height was about 0.787 mm with a copper thickness of 0.035 mm and a size of about 30 mm x 24.895 mm. The experimental set up for measurement of S parameter is shown in Figure 3.10. In the experiment, transmission and reflection coefficient are measured by Agilent N5230A vector network analyser with a standard X-band waveguide as receiver. The Figure 3.11 shows the comparison between simulated and experimental results of S11.

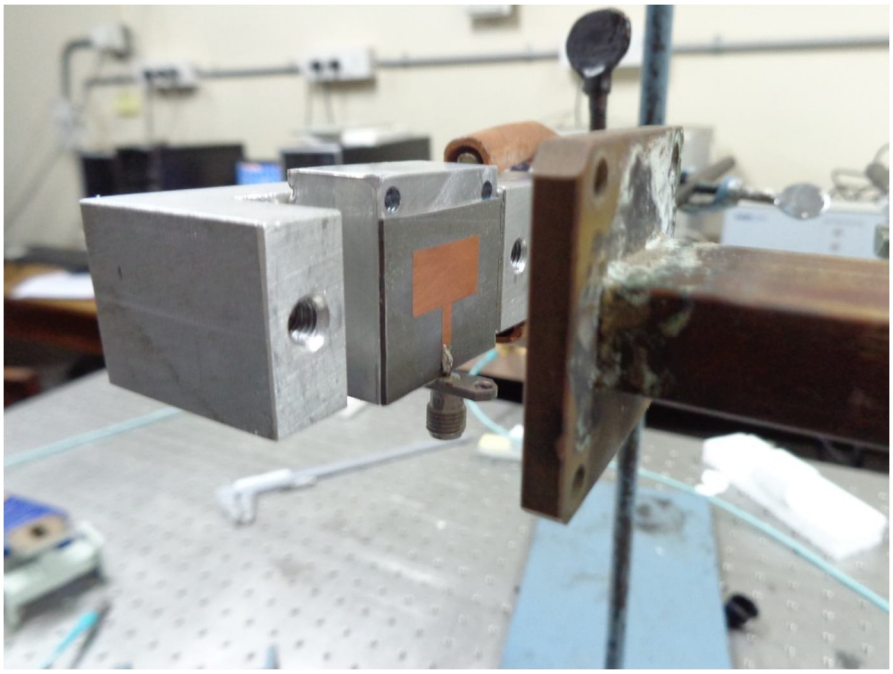

Figure 3.10: Experimental set up for measurement of S11 and S21 of patch antenna

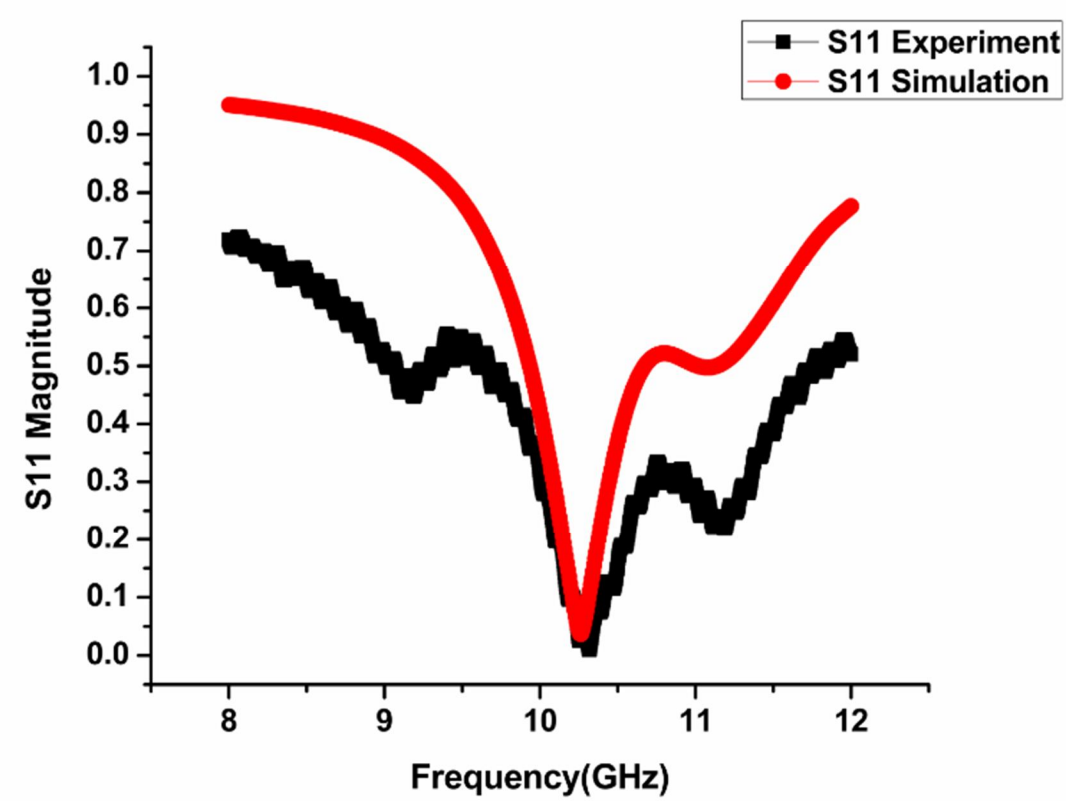

Figure 3.11: Comparison between simulated and experimental results of S11 of patch antenna

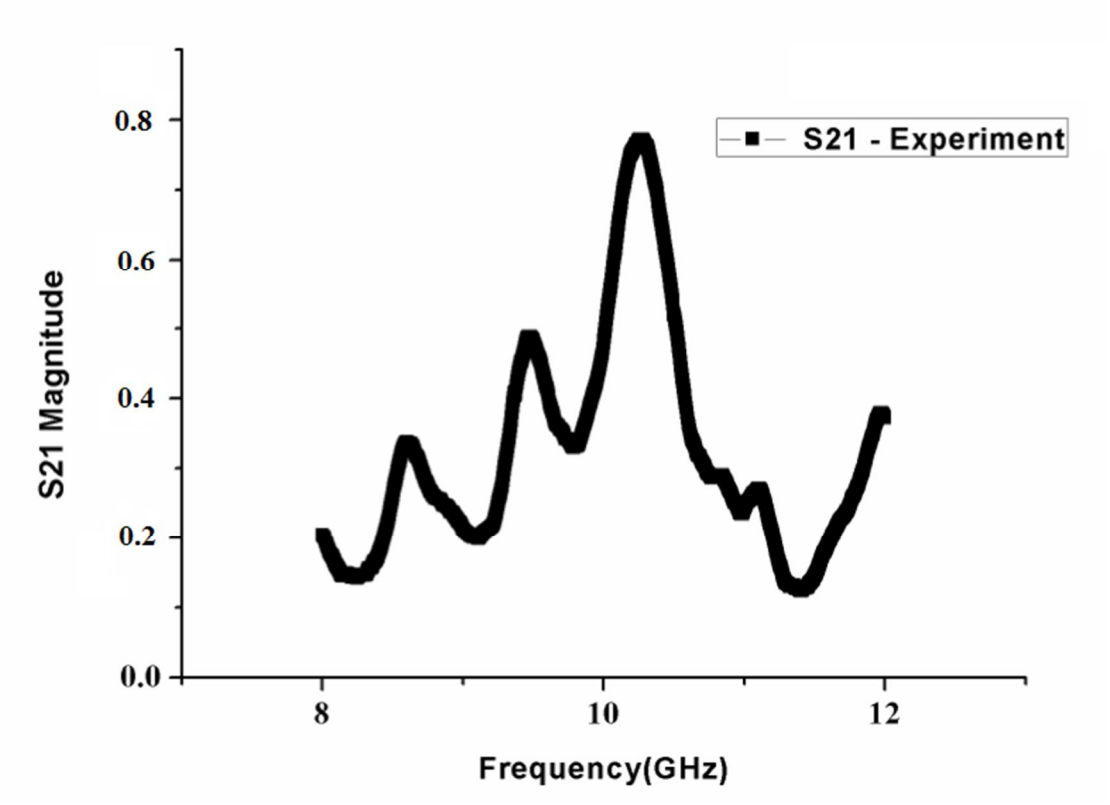

Figure3.12: Experimental result of S21 of patch antenna

From Figure 3.11, it is clear that the resonant frequency of the proposed structure is observed around 10.255 GHz with S11 in magnitude 0.0389 through the simulation, while the measured spectra shows resonance at 10.29 GHz with S11 magnitude 0.0299 which agrees with the simulated resonance frequency. It can also be seen from Figure 3.12 that, the transmission is maximum about 80% at the resonant frequency of 10.29GHz. Hence the simulated result is verified with experimental results and it is confirmed that the patch resonates at the designed frequency.

CHAPTER 4

DESIGN OF ZIM METAMATERIAL AS PATCH COVER

4.1 GENERAL EXPLANATION

A wave passing through a zero-index medium (ZIM) has a spatially uniform phase, characterized by a quasi-infinite wavelength. With the development of wave optics, the refractive index is now recognized as a measure describing the reduction of the speed and wavelength of light compared to their free-space counterparts, following the simple relations $v = c/n$ and $\lambda = \lambda_0/n$. (The frequency $\omega = 2\pi c/\lambda_0 = 2\pi v/\lambda$ doesn't vary in a "linear" optical material)[9]. In a general case where the wave has a propagation factor $e^{-i(\omega t - kz)}$, the refractive index (and consequently the wave vector , $k = \omega n/c$) assumes a complex value $n=n'+in''$, where $\exp(i2\pi n'z/\lambda_0)$ describes the phase advance the wave acquires during its propagation, and $\exp(-2\pi n''z/\lambda_0)$ gives the exponential decay of the field magnitude.

Within an ENZ (epsilon near zero) material, the wave exhibits little or no spatial variation, as the wavelength $\lambda = \lambda_0/n$ approaches infinity. The speed of light in the material, as indicated by $v = c/n$, becomes superluminal, posing an apparent contradiction to relativity. However, this velocity is the "phase velocity", which describes the rate at which the phase of the wave propagates. In contrast, the optical power or information travels at the "group velocity," which is limited by relativity, so causality still holds. Consequently, at zero index, $v_p \to \infty$ and $v_g \to 0$. In general, any material with $|n| < 1$ will be dispersive (with the index of refraction depending on wavelength), and any modulated signal in the material will travel below the speed of light in vacuum, albeit with a superluminal phase velocity for certain frequencies.

According to Snell's law, when the ray is incident from inside the low-index medium or zero-index medium (LIM/ZIM) into free space, the angle of refraction will be close to zero, and the refracted rays will be normal to the interface. This property provides a unique method of designing high-directive antennas.

4.2 PROPOSED STRUCTURE

The Figure 4.1 below shows the unit cell structure of the zero index metamaterial which has a plasma frequency of 10.255 GHz. The unit cell dimensions are w = 4mm, t = 1 mm, d= 0.787 mm, s = 3.5 mm, h = 16.6 mm and l = 10 mm.

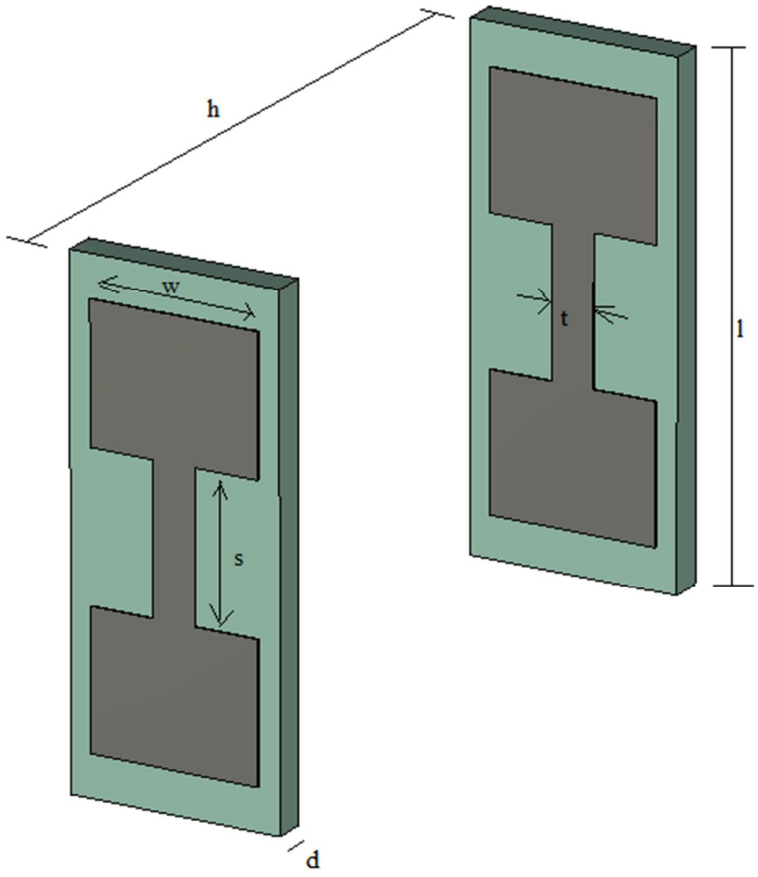

Figure 4.1: Unit cell structure simulated in CST microwave with dimensions marked.

This structure can be seen as a metallic thin-wire array. So the structure is characterized by a plasma frequency. The two-layer structure is excited by a plane wave, and the four sides of the structure are set to boundary conditions. These figures are shown as Figure 4.2 and 4.3.

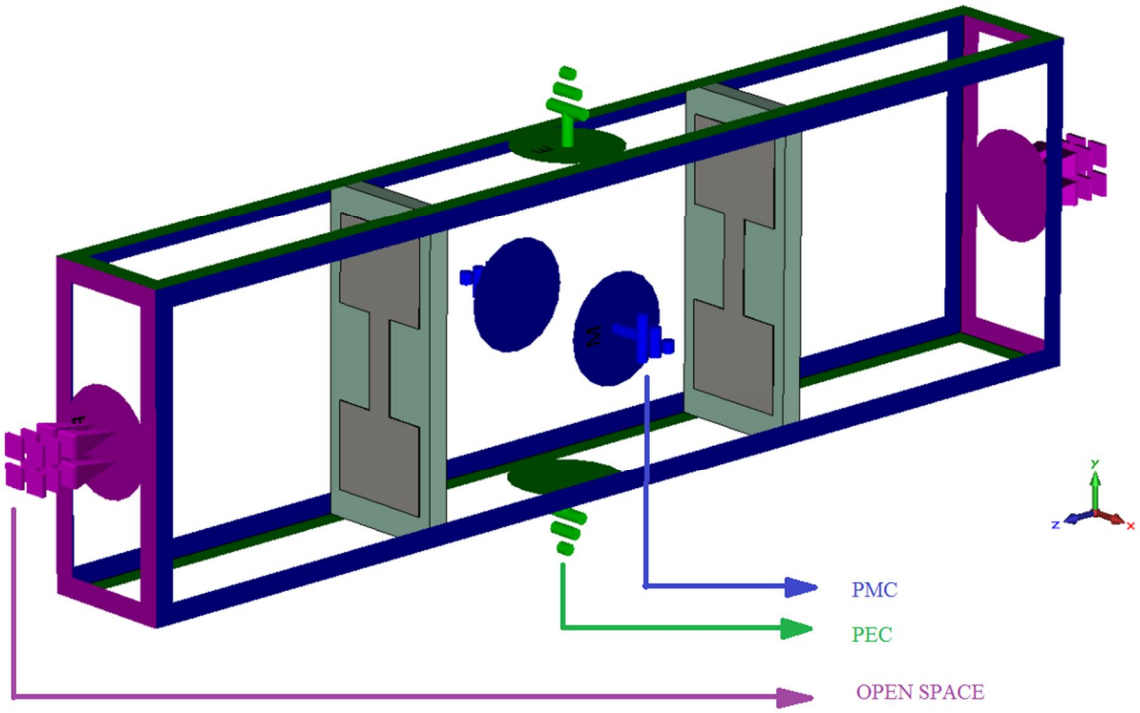

Figure 4.2: Blue: $H_t = 0$ (PMC), Green: $E_t = 0$ (PEC), Violet: Open space

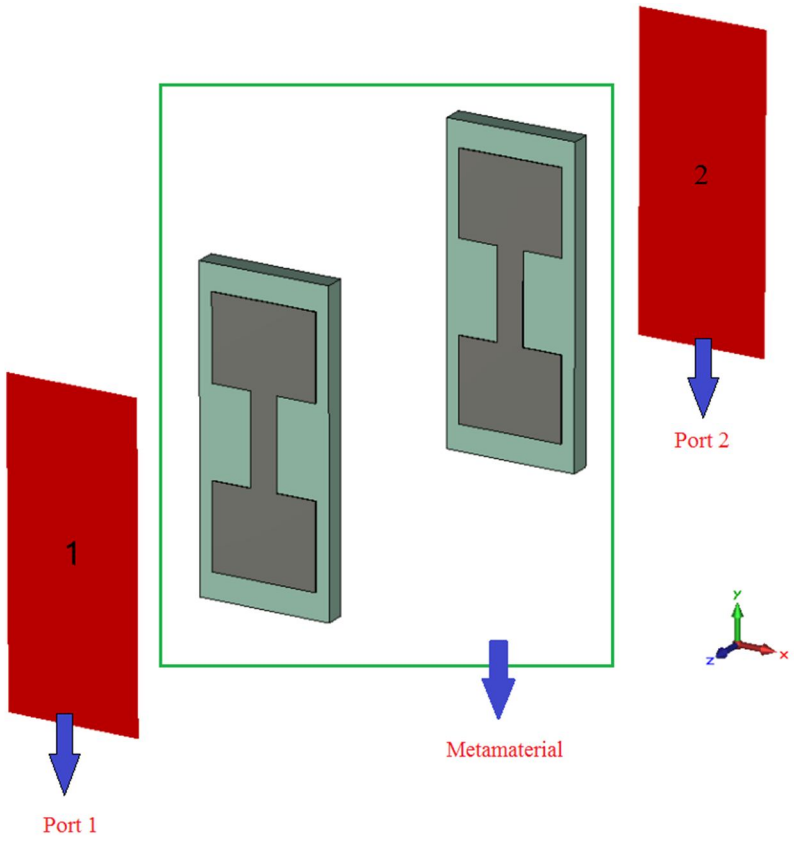

Figure 4.3: The two ports given for calculation of S parameters

4.3 S PARAMETER AND REFRACTIVE INDEX

The structure is simulated in CST Microwave Studio and S-parameters are obtained.

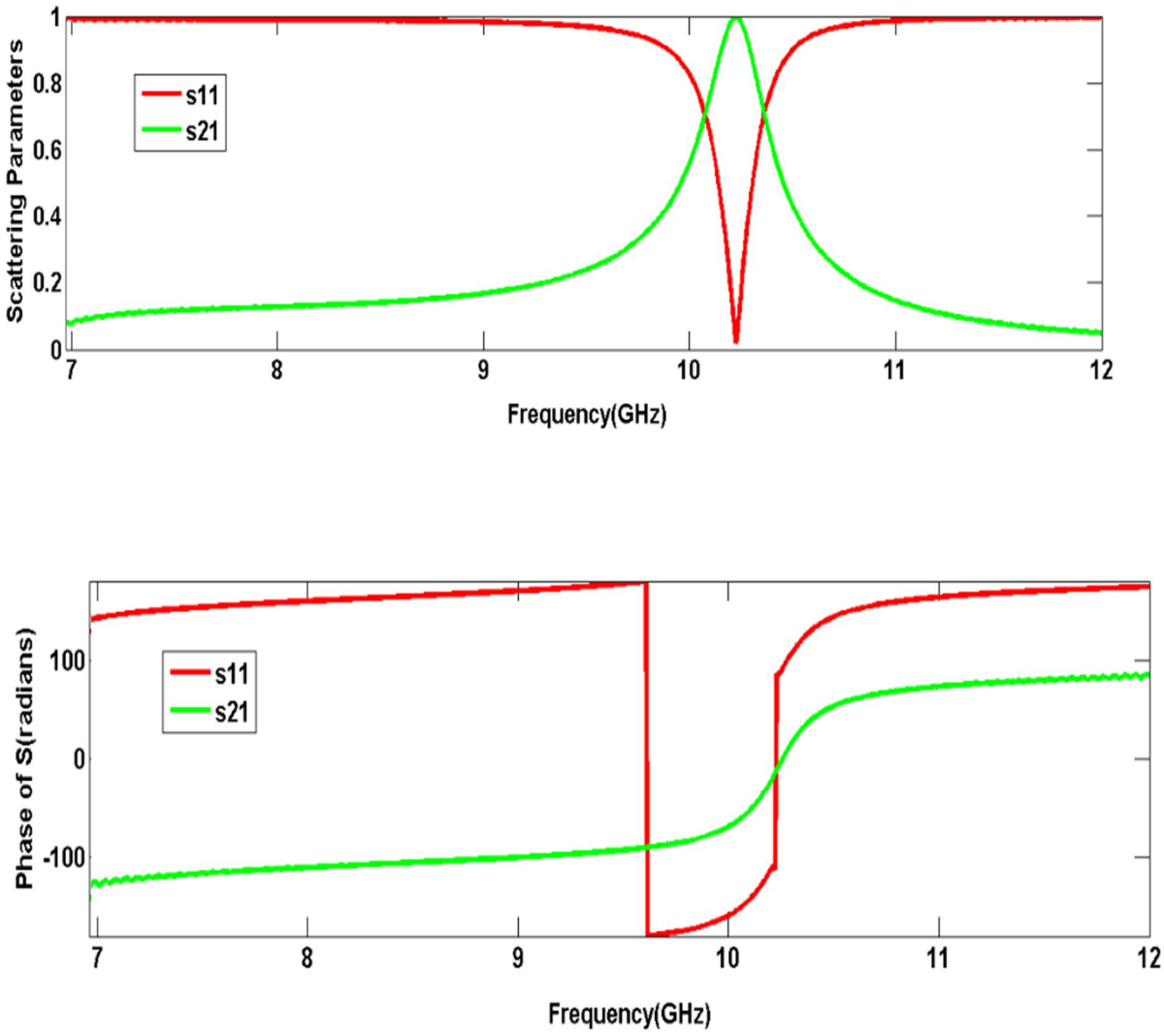

Figure 4.4: Magnitude and Phase of S11 and S21

The magnitude of S11 has minimum value of about 0.0009 and S21 has maximum value of 0.99 at 10.255 GHz, which is the plasma frequency. The phase of S11 and S21 shows a zero degree crossing at the same plasma frequency.

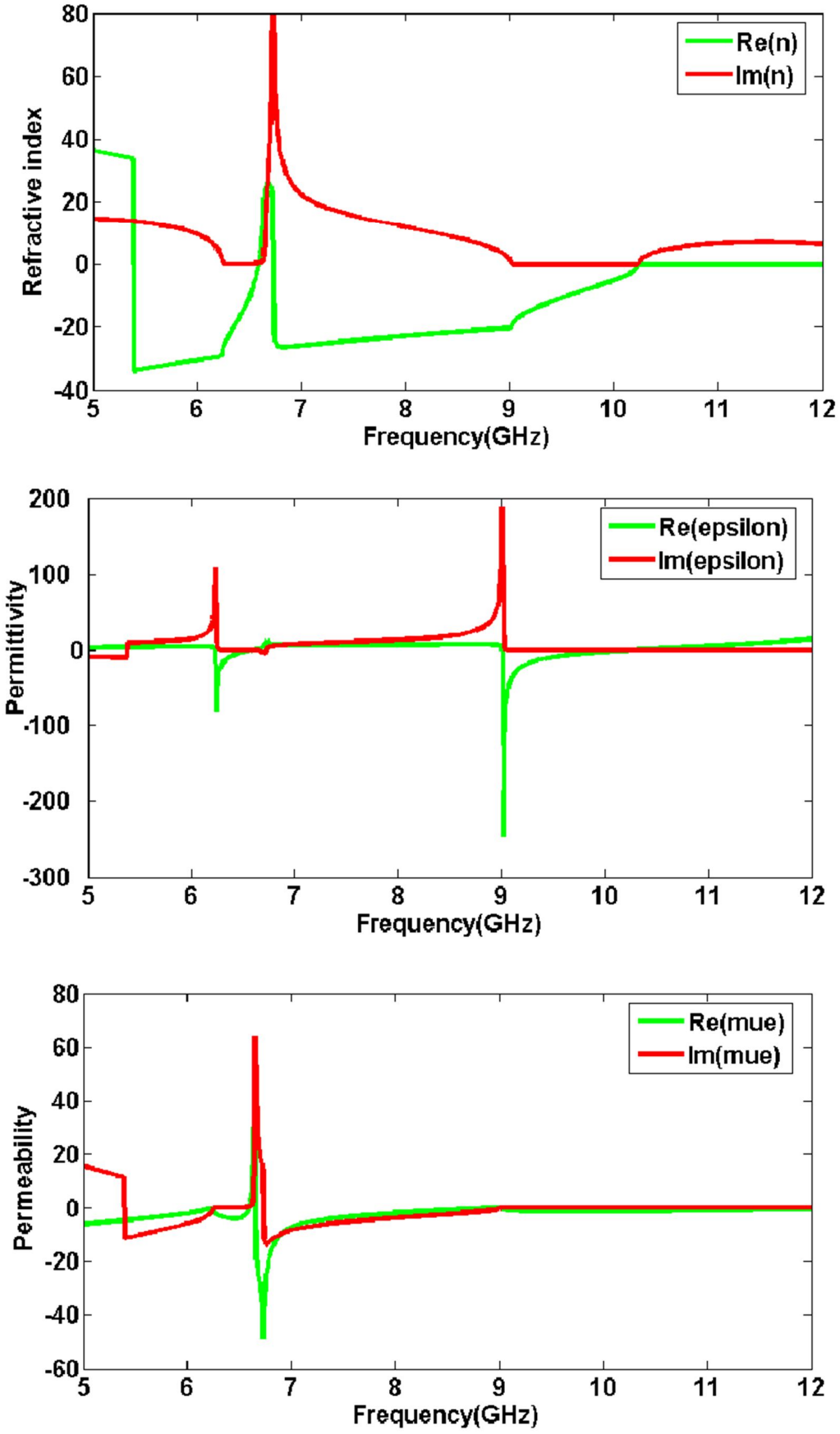

Figure 4.5: Refractive index, permittivity and permeability of metamaterial unit cell

It was found that at 10.255 GHz, both the real and imaginary parts of the effective permittivity are zero, which lead the refraction index at 10.255 GHz, very close to zero, for the unit cell. The structure is based on Rogers 5880 (lossy) substrate with loss tangent 0.0009. The unit cell was repeated with identical periodic metallic patterns printed on both sides of the substrate. The Rogers 5880 (lossy) substrate has a thickness of 0.787 mm and a dielectric constant of 2.2. The metallic pattern is as shown below in Figure 4.6.

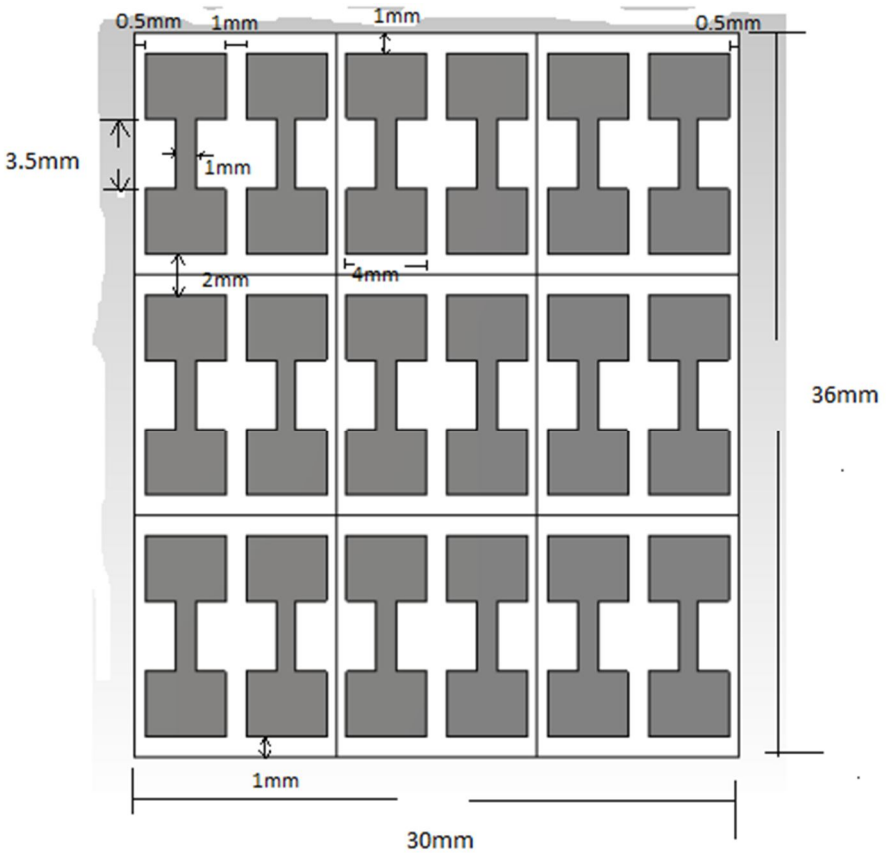

Figure 4.6: Metamaterial slab with repetition of unit cell

The size of the above metamaterial slab is 30 mm x 36 mm with Cu cladding thickness of 0.035 mm on both side of substrate.

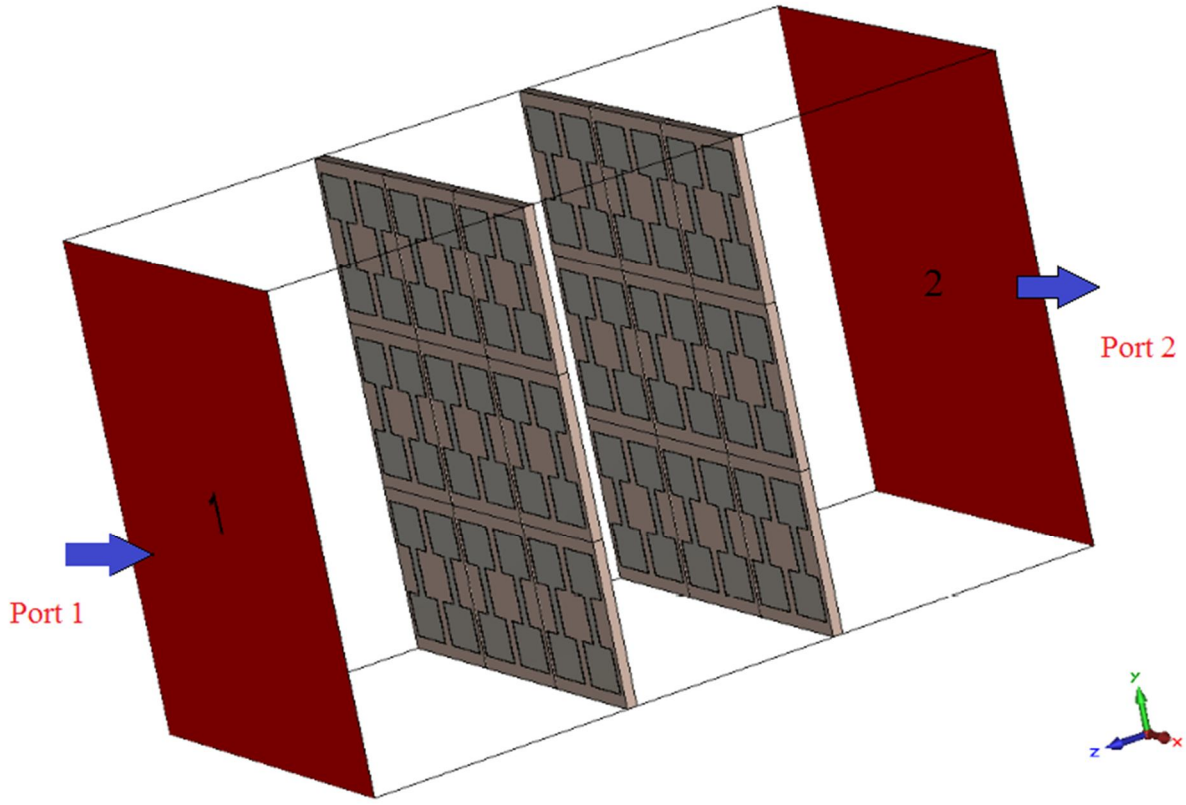

Figure 4.7: Simulated structure of metamaterial slab in CST Microwave Studio

The combined effect of the two slabs provides a near zero refraction around 10.255 GHz as similar as single unit cell.

In a zero-index medium (ZIM), the wave moves without changing its phase such that wavelength in medium becomes infinite. This can be identified by the propagation of electric field vector through the periodically arranged zero phase index metamaterial system with almost constant magnitude throughout the medium.

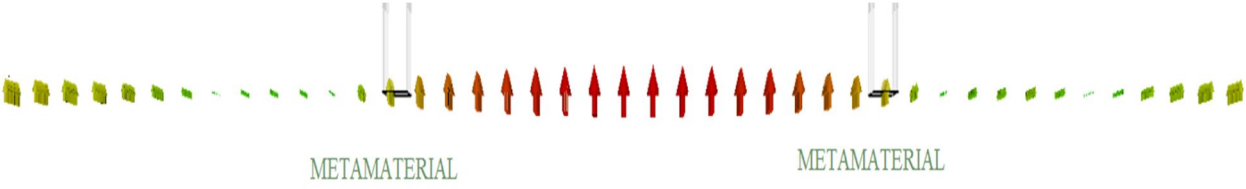

Figure 4.8: Electric field propagation through the metamaterial indicates constant phase inside the medium as the field arrows are not flipped upon many distances.

4.4 METAMATERIAL SUPERSTRATE FOR PATCH

The above zero-index metamaterial operating at 10.255 GHz is used as a superstrate over a patch designed at the same frequency. The substrate used for patch was Arlon Cu 233 LX (lossy) with dielectric constant 2.33 and loss tangent 0.0013. The length (L) and width of patch (W) were 8.847 mm and 17 mm respectively. Substrate height was about 0.787 mm with metal thickness of about t = 0.035 mm. The substrate size is 30 mm x 24.645 mm. The figure simulated in CST Microwave Studio is as shown below in Figure 4.9.

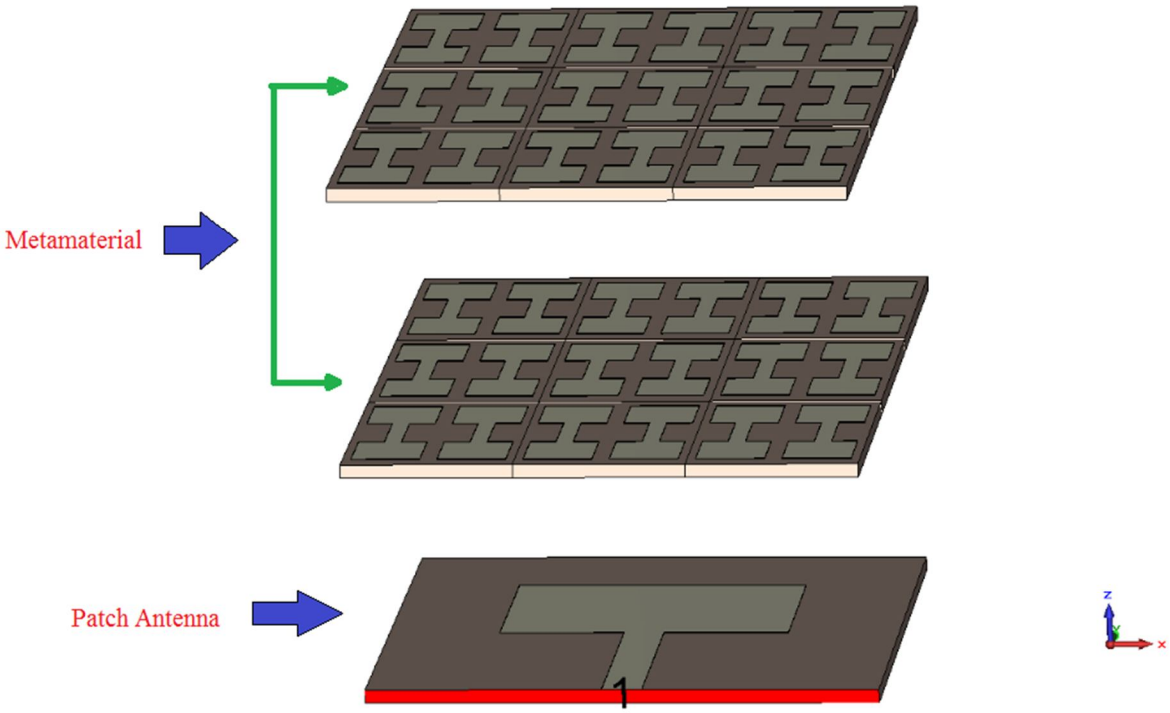

Figure 4.9: Simulation of metamaterial superstrate over patch antenna in CST Microwave Studio

Directivity will be improved when wave is coming out of the zero refracting medium in superstrate case. In superstrate case, the radiation pattern of an antenna is changed. Metamaterial nearly acts as a lens. So the beam is less diverging in the case of superstrate owing to the beam shaping comparing to the empty medium. Improvement in the directivity is good application of zero refractive index medium. As zero phase index refers infinite wavelength. It means the wavelength is very large for near zero phase

index. Since wavelength is very large (nearly infinite) we can say phase is constant. Here, metamaterial allows us to control the direction of emission of a source in order to collect all the energy in a small angular domain around the normal. Hence we are correcting the spherical wavefront coming out of the antenna through zero phase correction to increase directivity. The correction of spherical wave front to planar can be understood from the Figure 4.10 below.

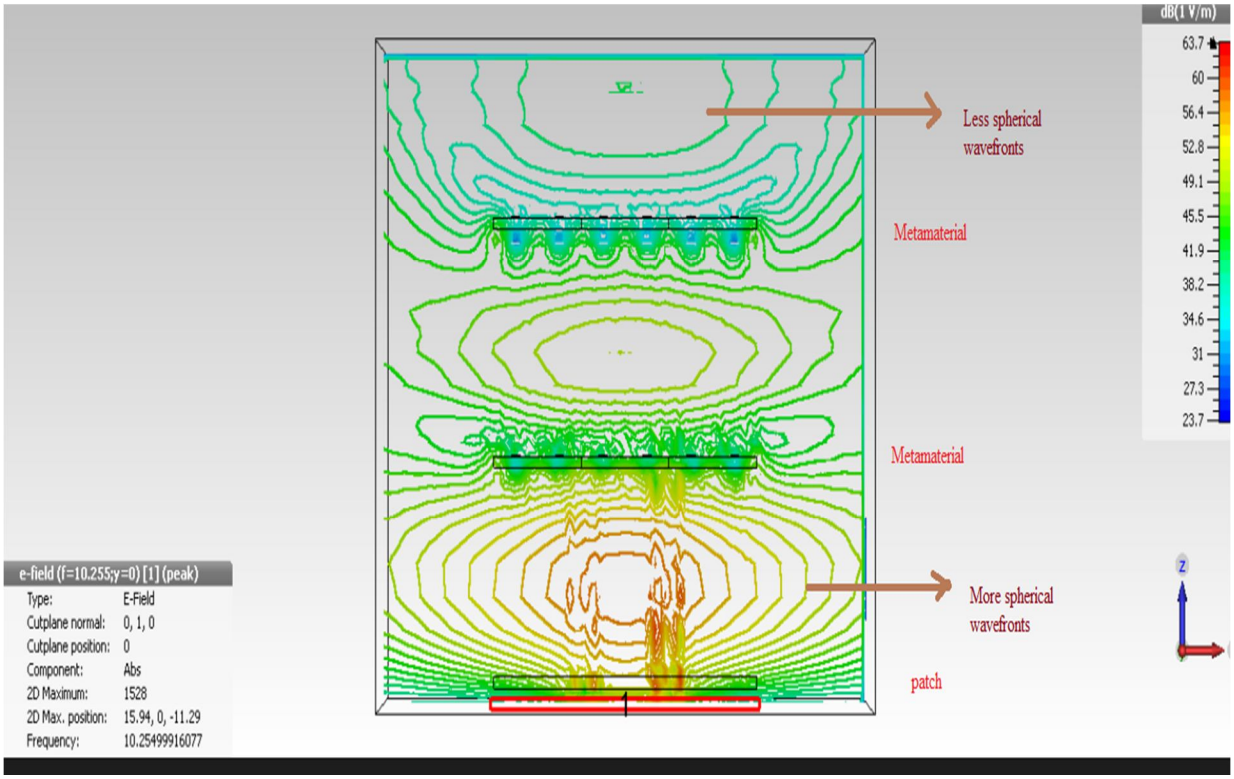

Figure 4.10: Correction of spherical wavefront to planar wavefront

From the Figure 4.10, it can be understood that the wavefront becomes less diverging after passing through the zero refracting metamaterial superstrate. That indicates the improvement in directivity of the patch antenna.

4.5 RADIATION PATTERN AND IMPROVEMENT IN DIRECTIVITY

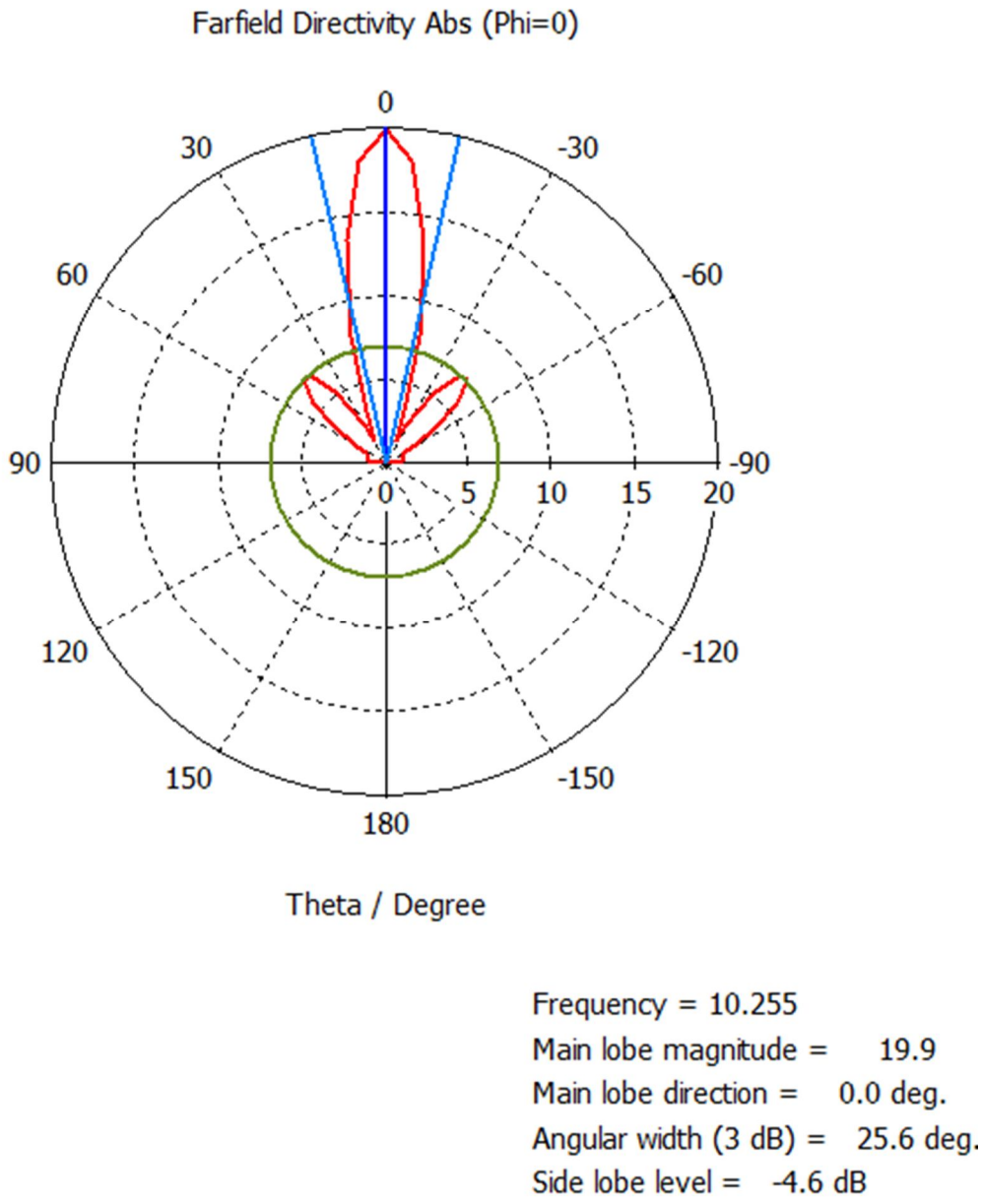

Figure 4.11: Elevation pattern of patch antenna with superstrate

The above Figure 4.11 shows the elevation pattern with 3dB angular width $\Delta\theta$ for patch antenna with superstrate. $\Delta\theta$ has decreased from 67.5^0 (without superstrate) to 25.6^0 (with superstrate).

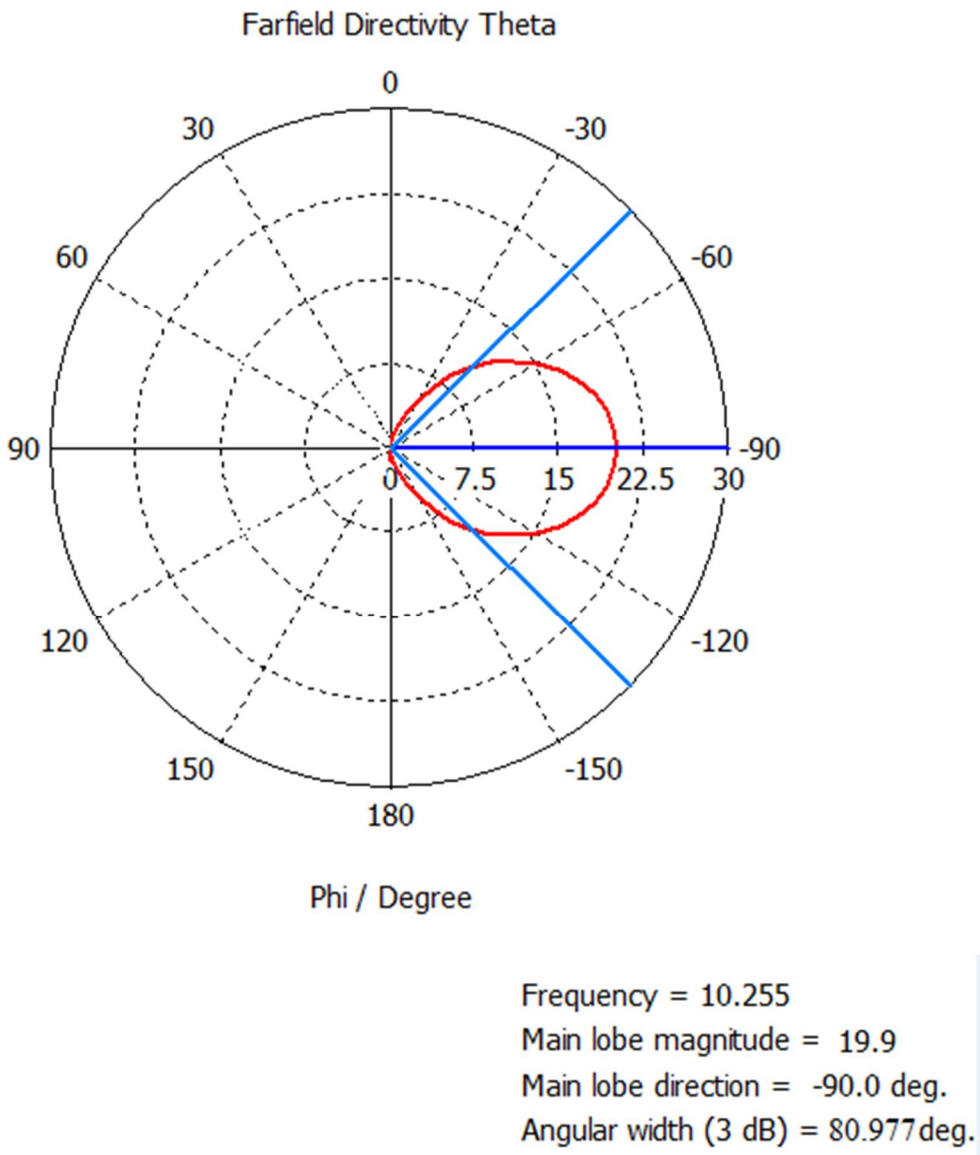

Figure 4.12: Azimuth pattern of patch antenna with superstrate

The above Figure 4.12 shows the azimuth pattern with 3dB angular width $\Delta\phi$ for patch antenna with superstrate. $\Delta\phi$ has decreased from 103.4^0 (without superstrate) to 80.977^0 (with superstrate). Directivity is improved from 7.68 dB to 13 dB, which is equal to improvement from 5.87 to 19.9 in linear scale.

4.6 VARIATION OF DIRECTIVITY WITH DISTANCE

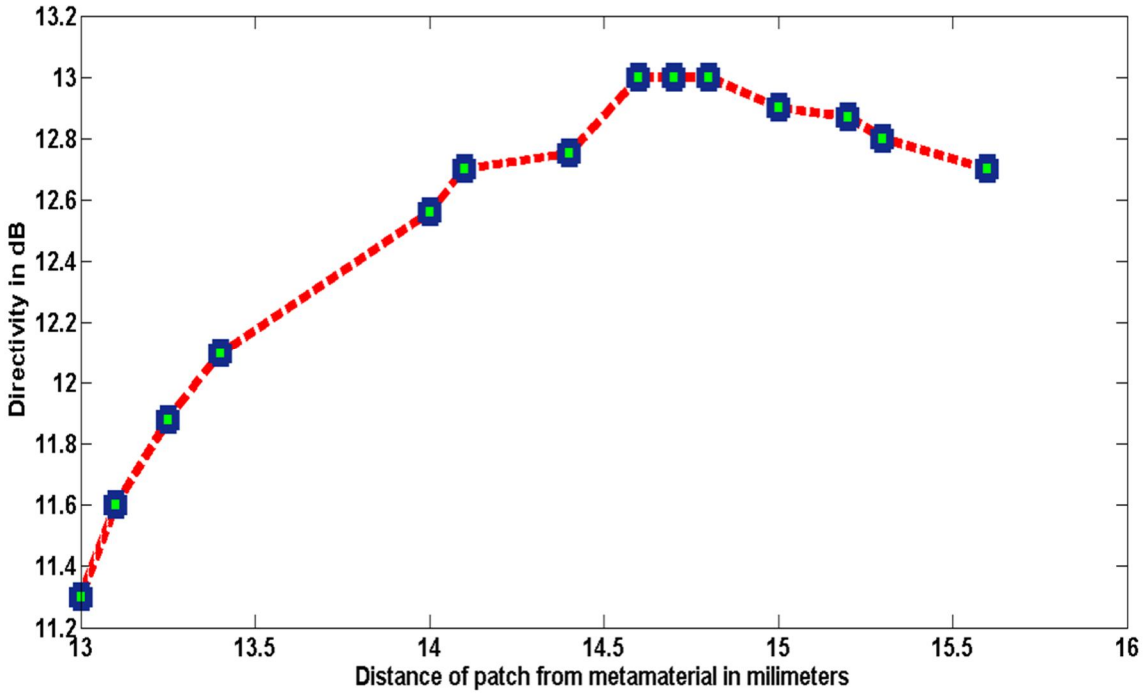

Figure 4.13: Variation of directivity of patch antenna with distance between antenna and superstrate

The above figure shows the variation in directivity of the antenna with the change in the distance between superstrate and patch. When the distance is about 14.6 mm (about λ/2), the directivity becomes maximum i.e. 13 dB.

Distance b/w superstrate & patch	Directivity(dB)
13	11.3
13.1	11.6
13.25	11.88
13.4	12.1
14	12.56
14.1	12.7
14.4	12.75
14.6	13
14.7	13
14.8	13
15	12.9
15.2	12.87
15.3	12.8
15.6	12.7

Table 4.1: Variation of Directivity with distance between superstrate and patch antenna

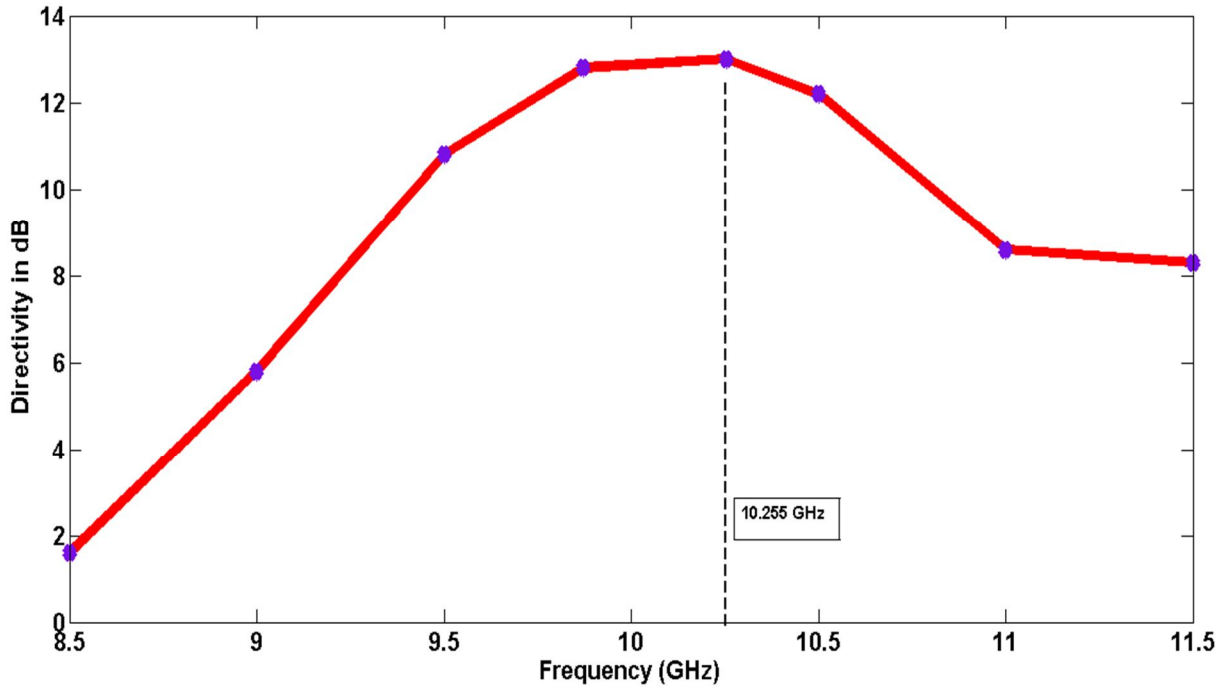

Figure 4.14: Variation of directivity (dB) of patch antenna with frequency

Frequency(GHz)	Directivity(dB)
8.5	1.6
9	5.8
9.5	10.8
9.872	12.8
10.255	13
10.5	12.2
11	8.6
11.5	8.3

Table 4.2: Variation of Directivity with frequency of operation

The above figure gives the variation of directivity of the antenna with frequency. It can be seen that, at 10.255 GHz, the directivity is maximum which is the operating frequency.

4.7 EXPERIMENTAL VERIFICATION

The simulated transmission of the electromagnetic wave is compared with the experimental results, which agrees well with the measured values of the transmitted field despite the fabrication and random errors in the measurements. The layout of the zero refractive index metamaterial structure is shown in Figure 4.15. It consists of 3X6 array of the unit cell structure patterned on the each side of the Rogers 5880 board of thickness 0.787 mm with a copper thickness of 0.035 mm and the dielectric constant of the board is 2.2 with loss tangent 0.0009.

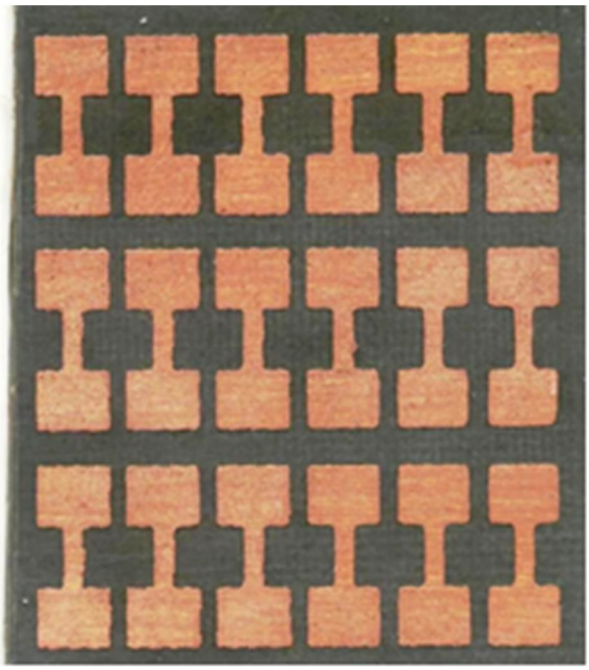

Figure 4.15: Fabricated board of the proposed structure

The experimental set up for the measurement of scattering parameter is shown in Figure 4.16. In the experiment, transmission and reflection coefficient are measured by Agilent N5230A vector network analyser with a standard X-band waveguide as transmitter and receiver. The two metamaterial structures are kept at an optimal distance of 16.6 mm and a linearly polarized electromagnetic wave is incident on the structure and on the other side of the structure, we measured the transmitted wave using a X-band waveguide, since the structure was small. The Figure 4.17 Figure 4.18 shows the comparison between simulated and experimental results of S11 and S21.

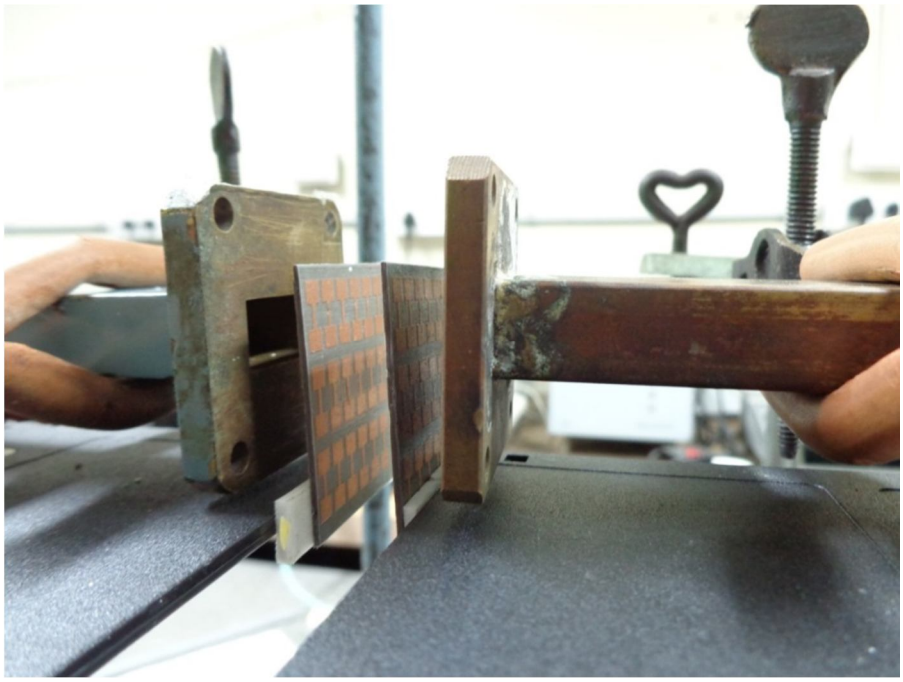

Figure 4.16: Experimental set up for measurement of S parameter for metamaterial

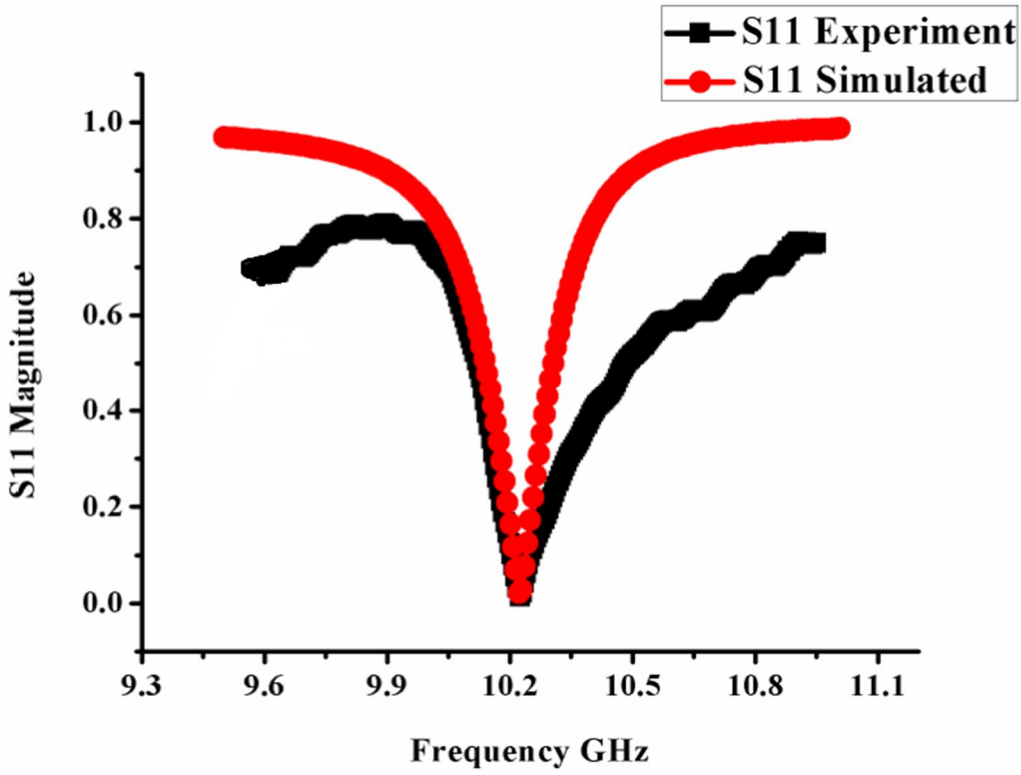

Figure 4.17: Comparison between simulated and experimental results of S11 of metamaterial

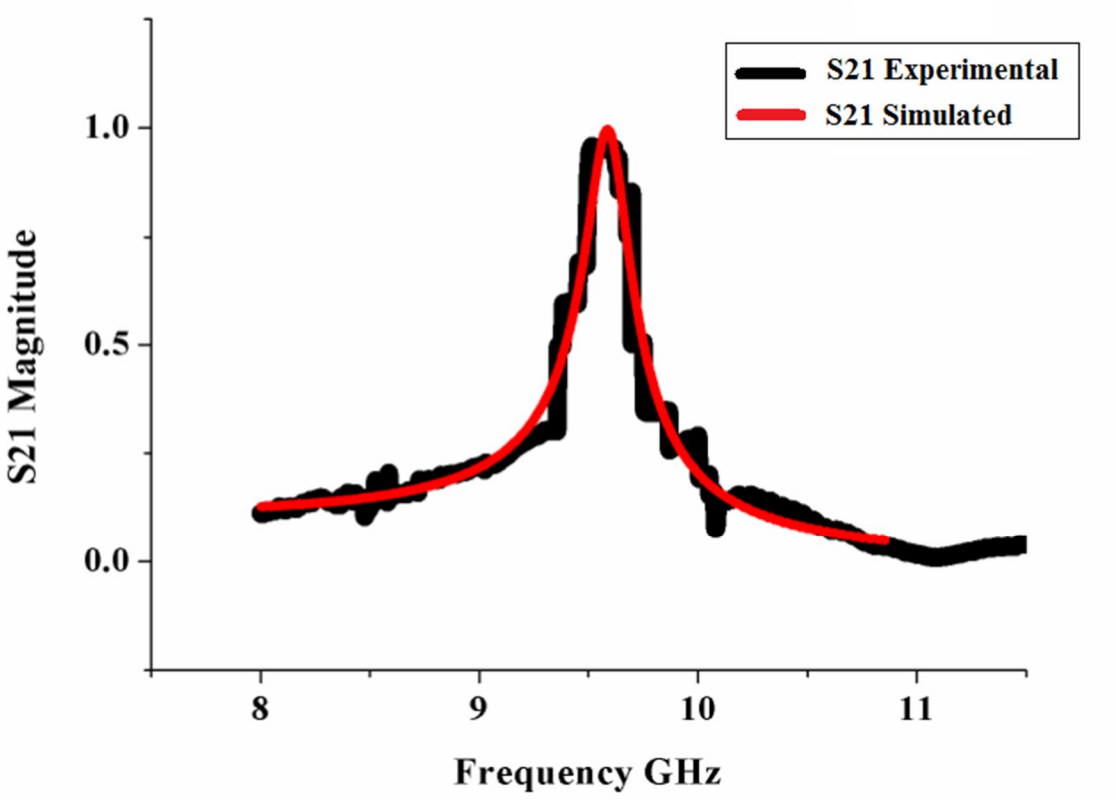

Figure 4.18: Comparison between simulated and experimental results of S21 of metamaterial

The simulated and measured results are comparable and agree well with each other. The resonant frequency of the proposed structure is observed around 10.255 GHz with S11 in magnitude 0.0009 through the simulation, while the measured spectra shows resonance at the same frequency with almost same S11 magnitude which agrees with the simulated resonance frequency. It can also be seen from Figure 4.18, that, the transmission is maximum almost 100% at the resonant frequency of 10.255 GHz. Hence the simulated result is verified with experimental results and it is confirmed that the resonant frequency at which metamaterial shows its zero refraction is 10.255 GHz. This structure is kept in front of patch antenna and again the S-parameter is found. The experimental set up for this is shown in the below Figure 4.19.

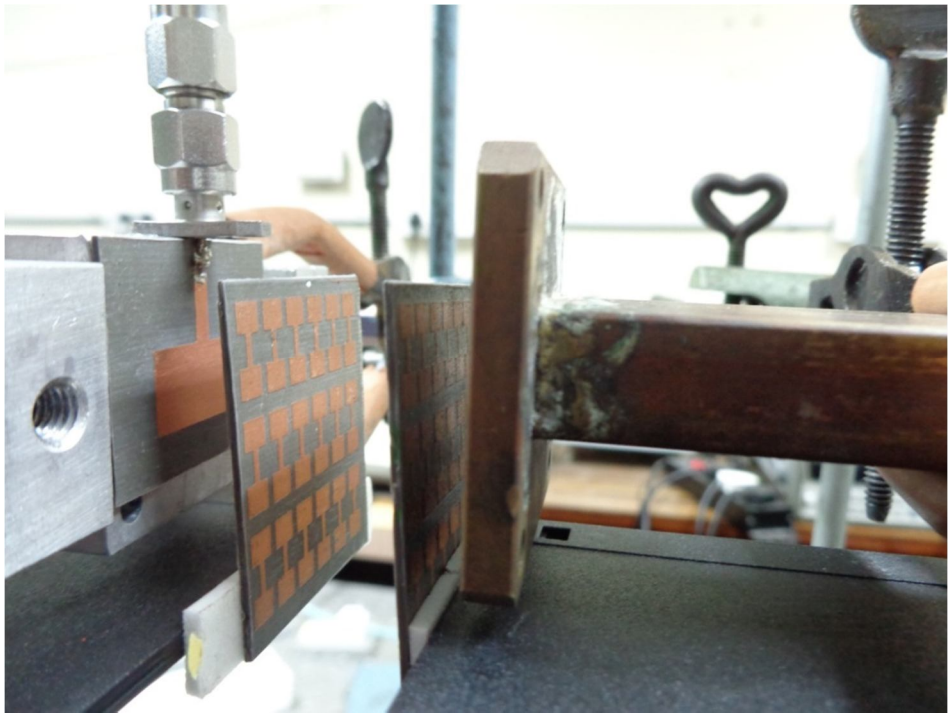

Figure 4.19: Experimental set up for measurement of S parameter for antenna with metamaterial

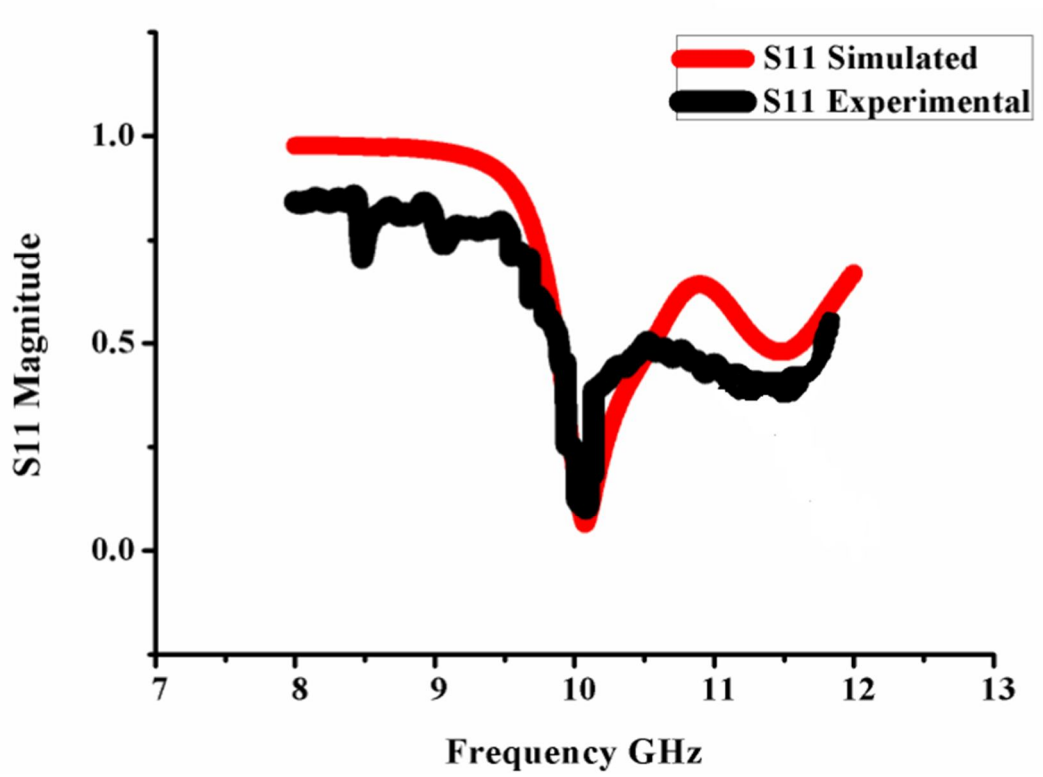

Figure 4.20: Comparison between simulated and experimental results of S11 of antenna with metamaterial

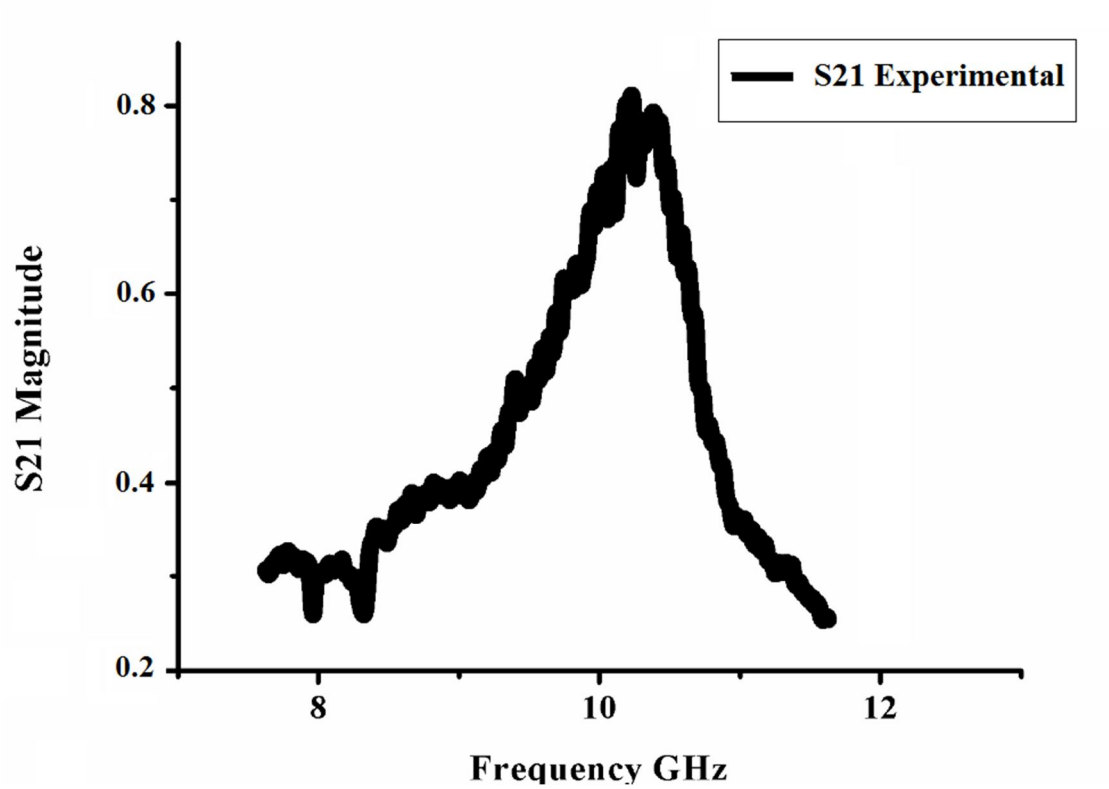

Figure 4.21: Experimental results of S21 of antenna with metamaterial

From Figure 4.20, it is clear that the resonant frequency of the proposed structure is observed around 10.255 GHz with S11 in magnitude 0.043 through the simulation, while the measured value shows resonance at the same frequency 10.255 GHz with S11 magnitude 0.051 which agrees with the simulated resonance frequency. It can also be seen from Figure 4.21 that, the transmission is maximum about 80 % at the resonant frequency of 10.255 GHz. Hence the simulated result is verified with experimental results and it is confirmed that the patch antenna with superstrate resonates at the designed frequency .This superstrate increases the directivity of patch antenna from 5.86 to 19.9 in linear scale, which was shown through simulation in detail before.

CHAPTER 5

DESIGN OF METAMATERIAL FOR ANTENNA BEAM STEERING

5.1 GENERAL EXPLANATION

Electronically scanned phased arrays are widely used in various civil and military applications including radar, broadcasting, cellular communications, satellite communications, and weather forecasting. However, the implementation of phased arrays has been limited to base stations, military applications, and high-end commercial products, regardless of their numerous technical advantages. The primary hindrance of the wide-scale deployment of phased arrays is the high cost associated with transmit/receive (T/R) modules. Phase shifters are critical elements within these T/R modules that create phase shifts between antenna elements and steer the antenna beam to the desired direction. In many cases, the cost of phase shifters is up to nearly half of the cost of an entire electronically scanned phased array [10]. Moreover these shifters are large and complex. There have been continued efforts in developing phase shifters using solid-state devices, microelectromechanical systems (MEMS) structures, or ferrite materials. Nevertheless, the cost of phase shifters using all these techniques is still too high for phased arrays to be widely used in low-end commercial products in the foreseeable future. Therefore, there is an immense need to develop next generation ultralow cost phased arrays using novel approaches.

In this thesis, a new scheme to utilized realize beam steering antenna, in which the beam is steered by a metamaterial-based active radom which is simpler and economical. The phase shift is achieved by varying the refractive index of the metamaterial structure. Larger refractive index results in larger phase shift, thus larger beam-steering angle. By inserting some lumped elements like variable capacitors or inductors into these metamaterial structures, the left-handed properties of these metamaterials can be electrically controlled for steering the beam of microstrip patch antenna. Thus a phase-controlled radom can be obtained to realize a steering antenna system without employing traditional complex microwave feeding network.

5.2 PROPOSED STRUCTURE

The Figure 5.1, below shows the unit cell of a omega-type metal inclusion which acts as a varying index metamaterial depending on the variable capacitance connected to its gap. The substrate used for the metamaterial is having a dielectric constant of 4.0 with a loss tangent of about 0.02. The thickness of the substrate is about 0.8 mm with a basic cell dimension of **R**=1.1 mm, **g** = 0.5 mm, **w** = 0.5 mm. The substrate is 3.9 mm along the x and y directions, 0.8 mm along z.

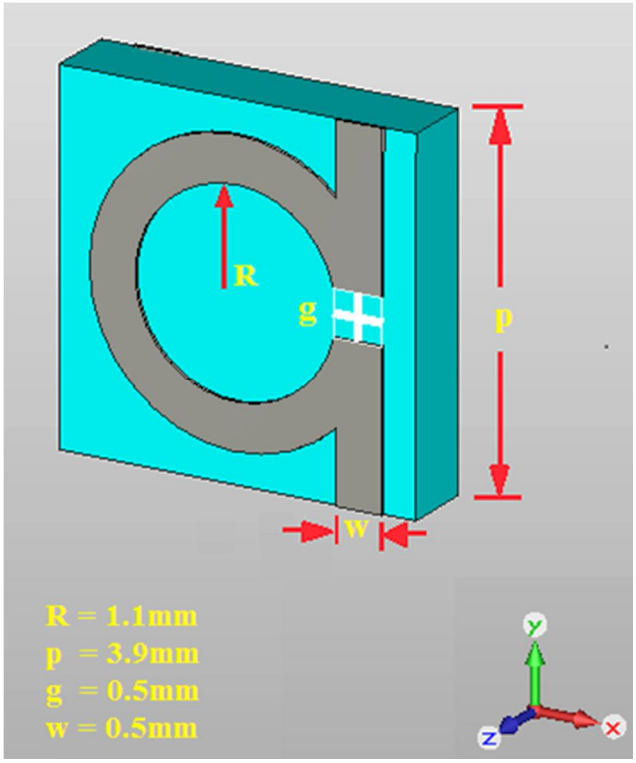

Figure 5.1: Geometry of the Omega pattern

The basic unit cell is composed of two Ω patterns in a back-to-back configuration as shown in figure 5.2. The two omega metallic pattern has a copper cladding thickness of 0.035 mm. For pure magnetic excitation, namely for a magnetic dipole induced by the incident magnetic field **H**, the orientation of the magnetic field is along the **z** axis which is collinear to the axis of the split ring of the unit cell. In addition, in order to induce an electrical activity, the **E** field is oriented along **y** axis which is parallel to the arms of the omega patterns and the propagation of electromagnetic wave is along **x** axis. The plasma frequency ω_p of this structure is inversely proportional to the square root of inductance and capacitance of the C loops.

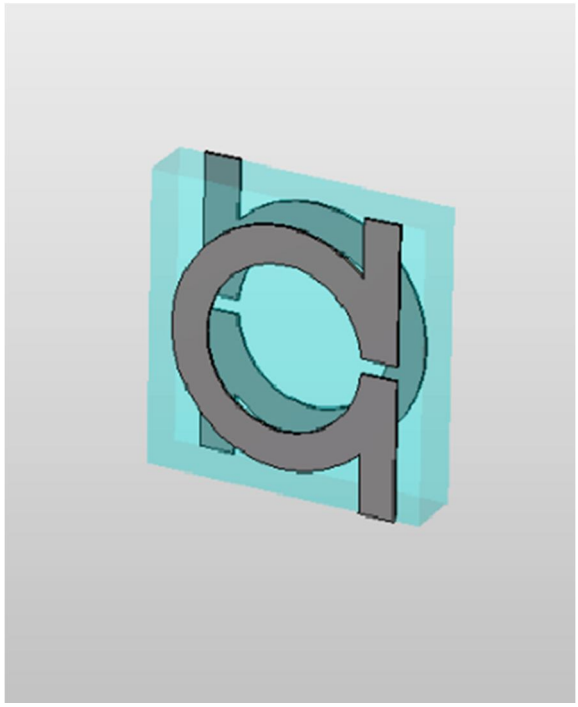

Figure 5.2: Back to back configuration

By connecting a variable capacitor across the gap (**g**) of the two omega (Ω) patterns, the plasma frequency of the structure can be varied. By adding a variable capacitor C to the gap, the net capacitance adds up since its effect is that of parallel connection. The shifting of plasma frequency can be understood from the S parameter curve. The structure is excited by a plane wave, and the four sides of the structure are set to boundary conditions. These figures are shown as Figure 5.3 and 5.4.

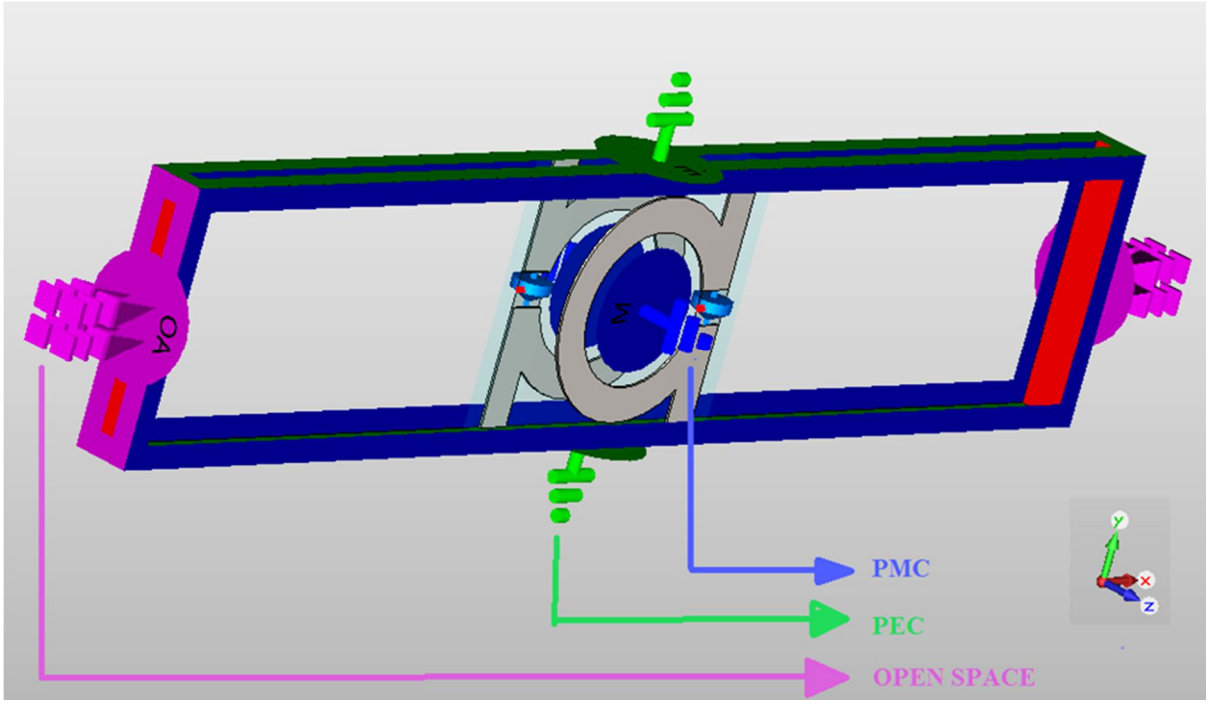

Figure 5.3: Blue: H_t =0 (PMC), Green: E_t =0 (PEC), Violet: Open space

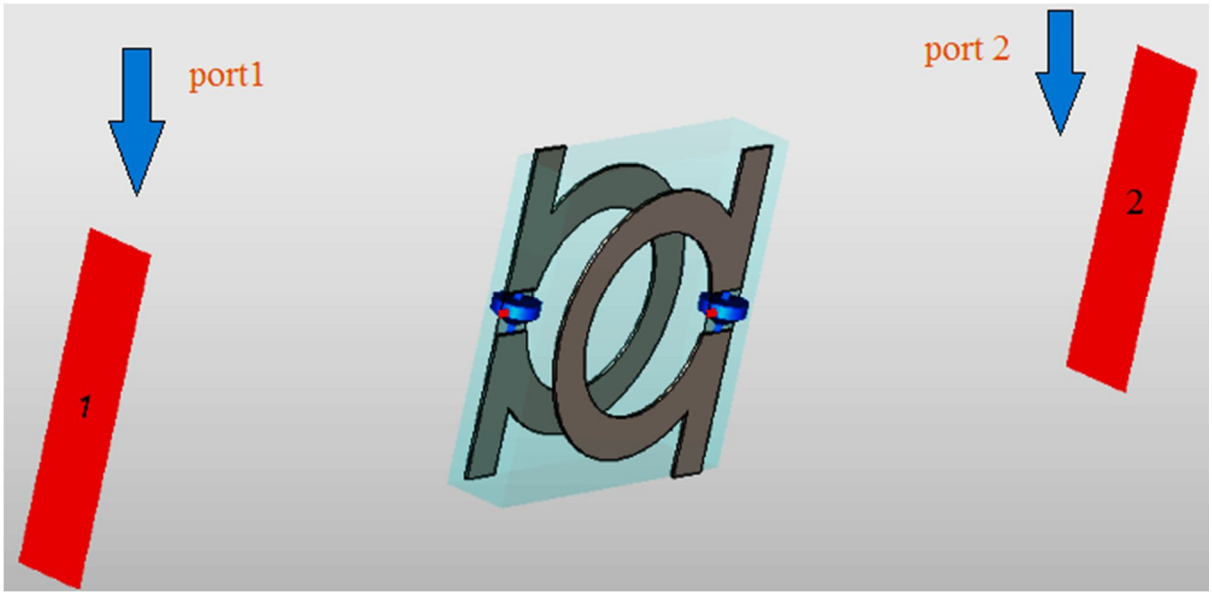

Figure 5.4: Simulation of metamaterial superstrate over patch antenna in CST Microwave Studio

The incident electromagnetic wave is given to port 1, which gets transmitted through the material and reaches port 2. This type of arrangement is used to find the S-parameter of the structure using CST Microwave studio.

5.3 S PARAMETER AND REFRACTIVE INDEX

From the below figure (Figure 5.5), it can be clearly identified that as the variable capacitance C is varied, the plasma frequency ω_p varies. As C is increased, plasma frequency decreases.

Variable Capacitance (C)	Plasma frequency (ω_p)	S11 in dB
0.3 pF	10.61 GHz	-20.013 dB
0.8 pF	9.75 GHz	-20.534 dB
1.6 pF	9.11 GHz	-20.995 dB

Table 5.1: Variation of S11 with variable capacitance

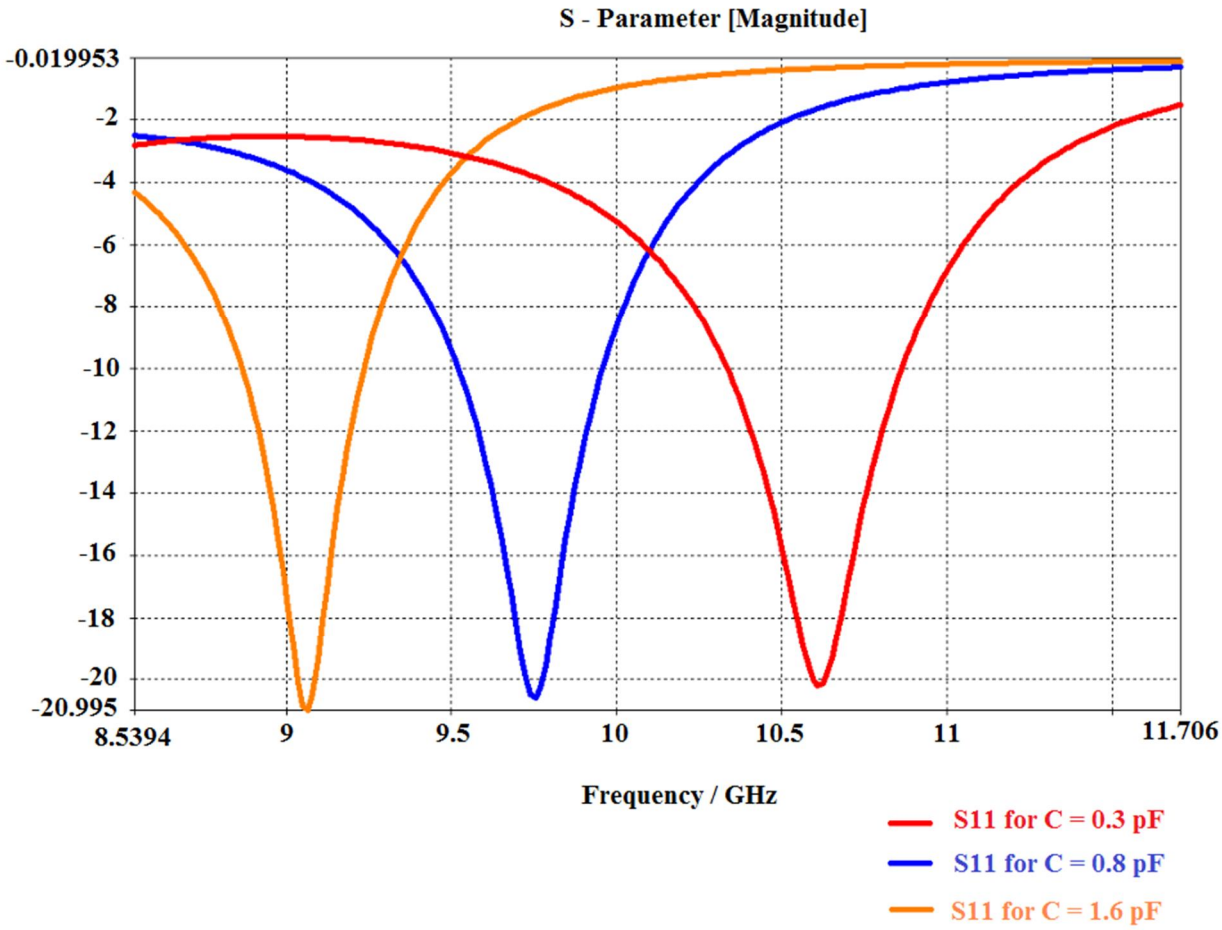

Figure 5.5: Variation of S11 of the metamaterial with variable capacitor

The refractive index can be extracted as per the parameter retrieval method explained in Chapter 2. The refractive index plot corresponding to each capacitance value is plotted in Figure 5.6 to Figure 5.8. As the capacitance value increases from 0.3 pF to 1.6 pF, the refractive index plot shifts from right to left. This can be seen as the zero refraction point shifts from 10.61 GHz to 9.11 GHz as variable capacitor is changed from 0.3 pF to 1.6pF.

Variable capacitance (C)	**Plasma frequency (ω_p)**	**Refractive index**
0.3 pF	10.61 GHz	0.00642
0.8 pF	9.75 GHz	0.00374
1.6 pF	9.11 GHz	0.0016

Table 5.2: Variation of Refractive index with variable capacitance

The unit cell structure of the back to back omega (Ω) pattern is repeated such a way that the arms of the omega pattern are interconnected along the y direction. This is shown in Figure 5.9. The unit cell is repeated as 3 X 3 array with a Cu cladding thickness of about 0.035 mm. The figure below (Figure 5.10) shows the metamaterial slab simulated in CST microwave studio. Here port 1 is the incident port and port 2 is the transmitting port. The S-parameter of this repeated back to back omega (Ω) pattern is same as that of unit cell. Hence, the refractive index of the pattern varies in accordance with the tuning capacitor.

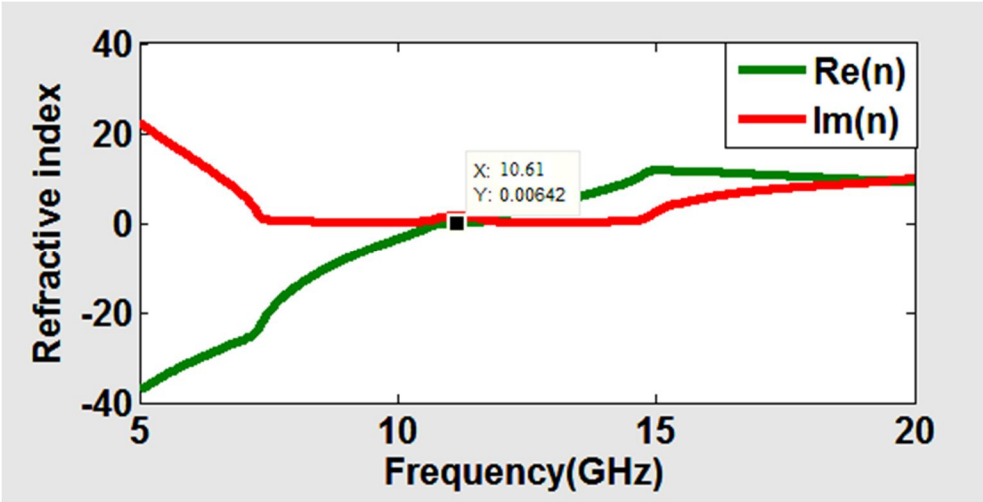

Figure 5.6: Refractive index of the metamaterial Vs frequency for C = 0.3 pF

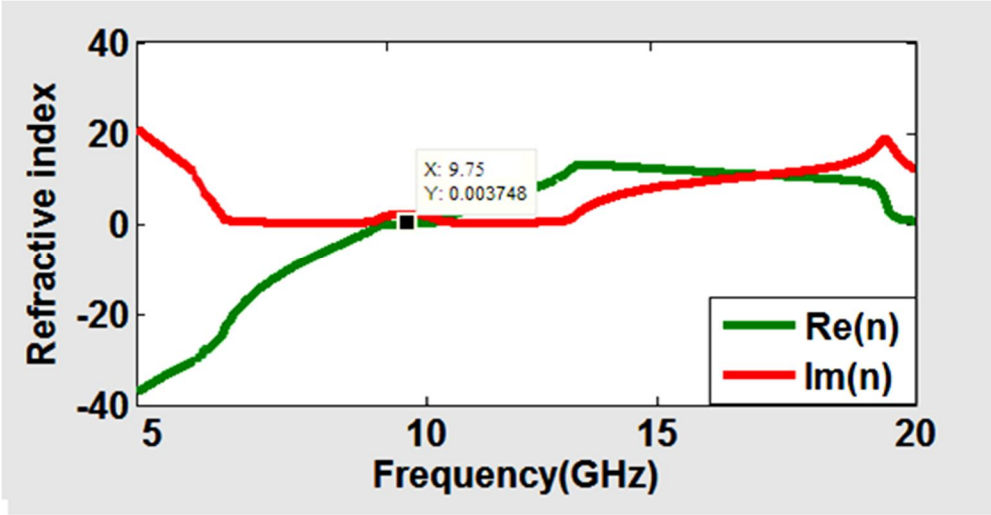

Figure 5.7: Refractive index of the metamaterial Vs frequency for C = 0.8 pF

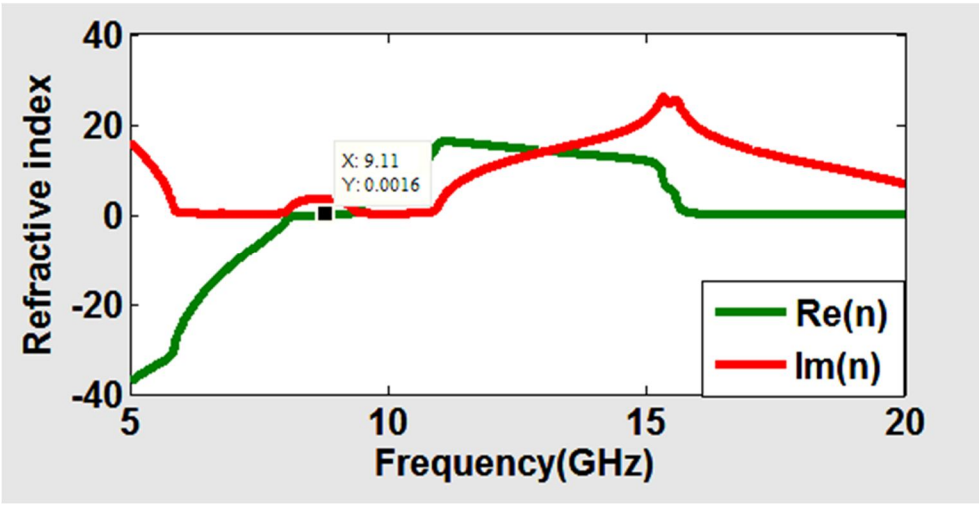

Figure 5.8: Refractive index of the metamaterial Vs frequency for C = 1.6 pF

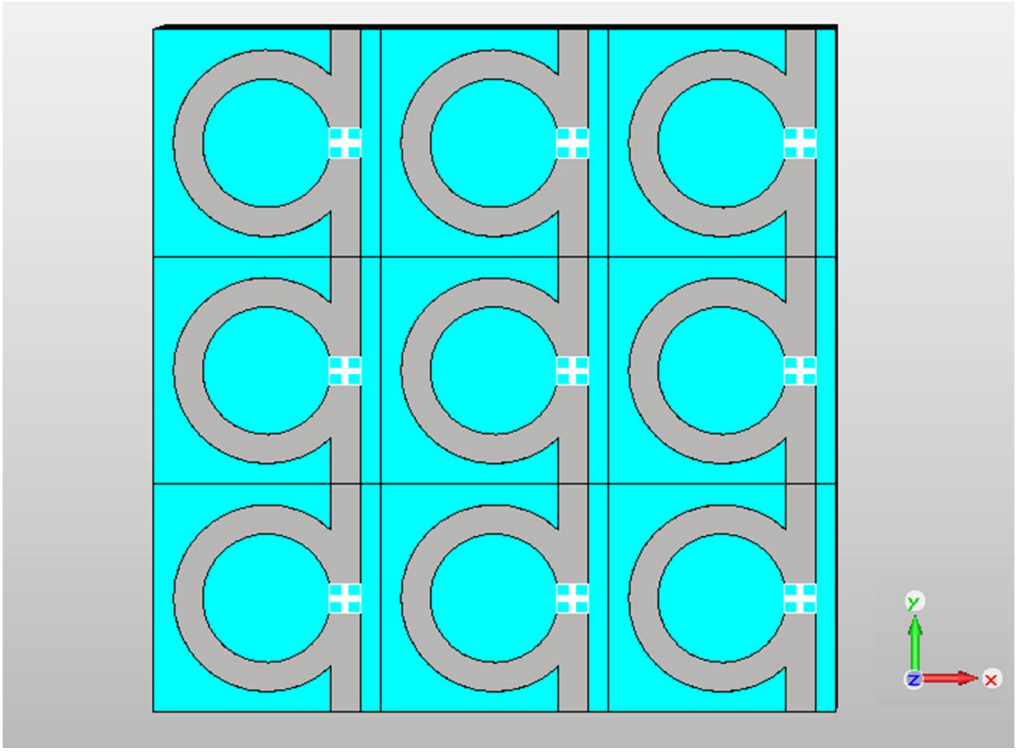

Figure 5.9: Metamaterial slab with repetition of unit cell

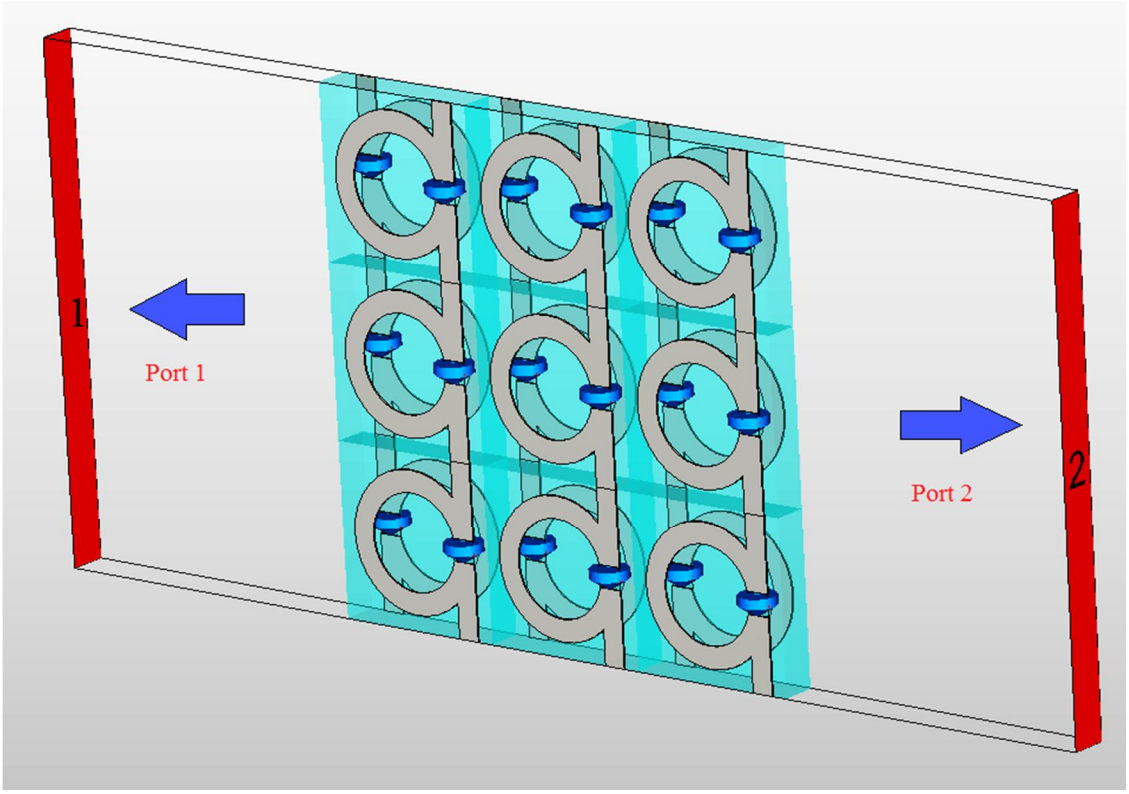

Figure 5.10: Simulated structure of metamaterial slab in CST Microwave Studio

5.4 VARIATION OF REFRACTIVE INDEX AT A PARTICULAR FREQUENCY

From the refractive index plots in Figure 5.11 to Figure 5.13, it is clear that the refractive index values vary as variable capacitor C varies. Since the refractive index graph shifts from right to left as capacitance value increases from 0.3 pF to 1.6 pF, the value of refractive index becomes less negative. For higher values of capacitance, the refractive index values become more and more positive. This is shown in Table 5.3 below.

Variable Capacitance (C)	**Plasma frequency (ω_p)**	**Refractive index at 9.4GHz**
0.3 pF	10.61 GHz	-6.134
0.8 pF	9.75 GHz	-3.252
1.6 pF	9.11 GHz	1.962

Table 5.3: Variation of Refractive index at 9.4 GHz with variable capacitance

When an electromagnetic wave of frequency 9.4 GHz passes through this omega structure with varying capacitance, the wave experiences different phase shifts each time when the refractive index varies. This can result in steering the beam in different direction according to varying capacitance.

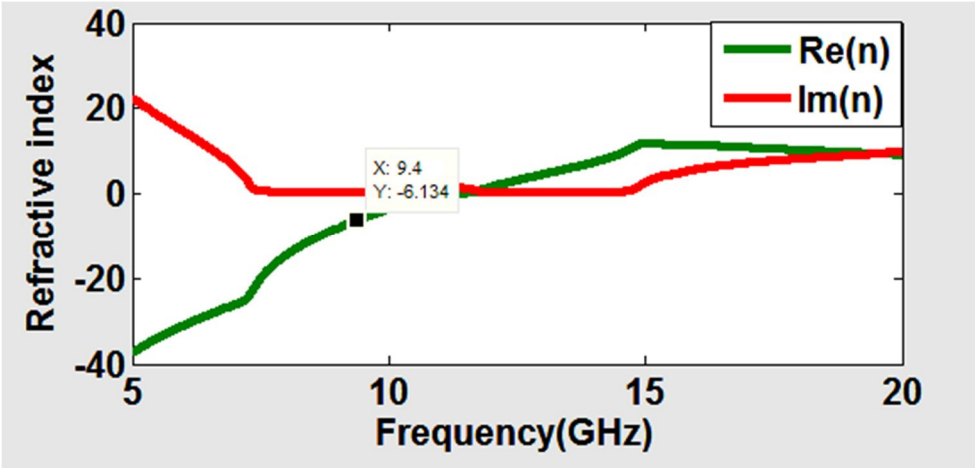

Figure 5.11: Refractive index highlighted at 9.4 GHz for C = 0.3 pF

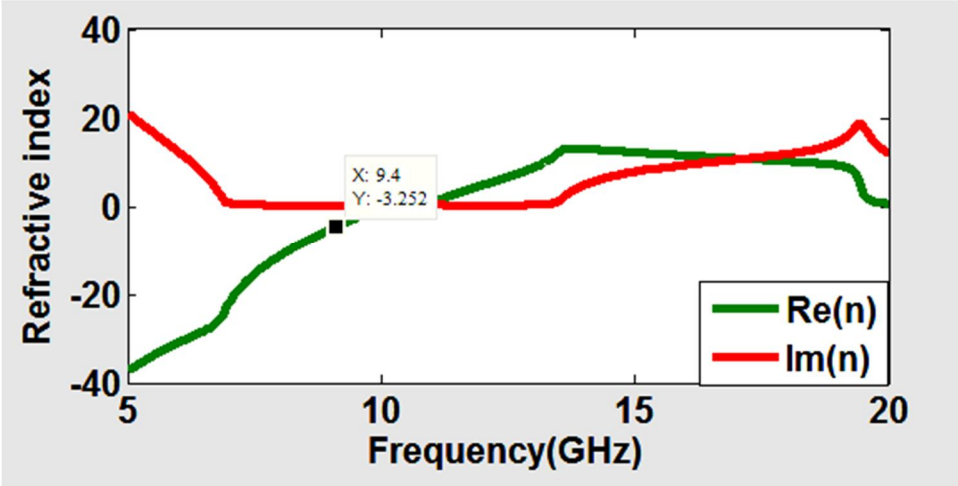

Figure 5.12: Refractive index highlighted at 9.4 GHz for C = 0.8 pF

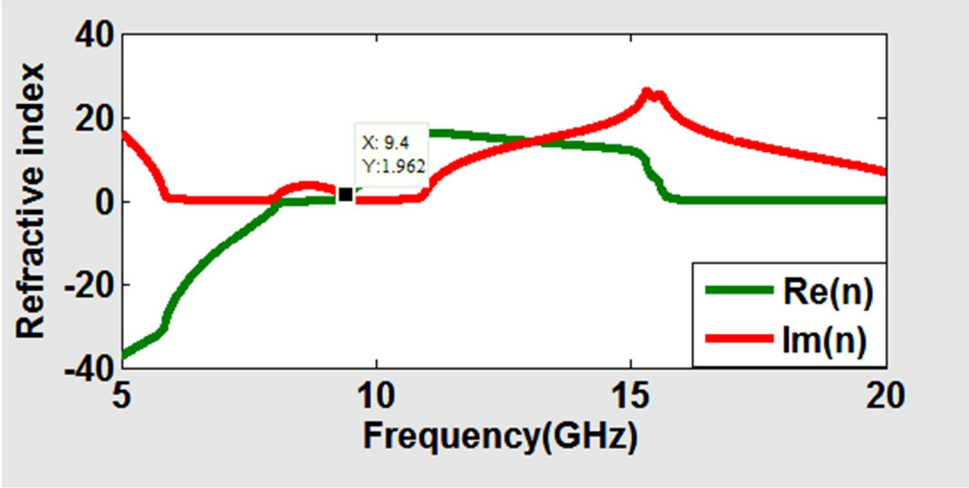

Figure 5.13: Refractive index highlighted at 9.4 GHz for C = 1.6 pF

5.5 PATCH ANTENNA WITH RESONANT FREQUENCY 9.4 GHz

A microstrip patch antenna is designed for a resonant frequency of 9.4 GHz. The structure dimension is as shown below in Figure 5.14. The substrate used has a dielectric constant 2.2 and loss tangent 0.0009. The length (L) and width of patch (W) were 9.7 mm and 18 mm respectively. Substrate height was about 0.787 mm with metal thickness of about t = 0.035 mm. The substrate size is about 30 mm x 25.68 mm.

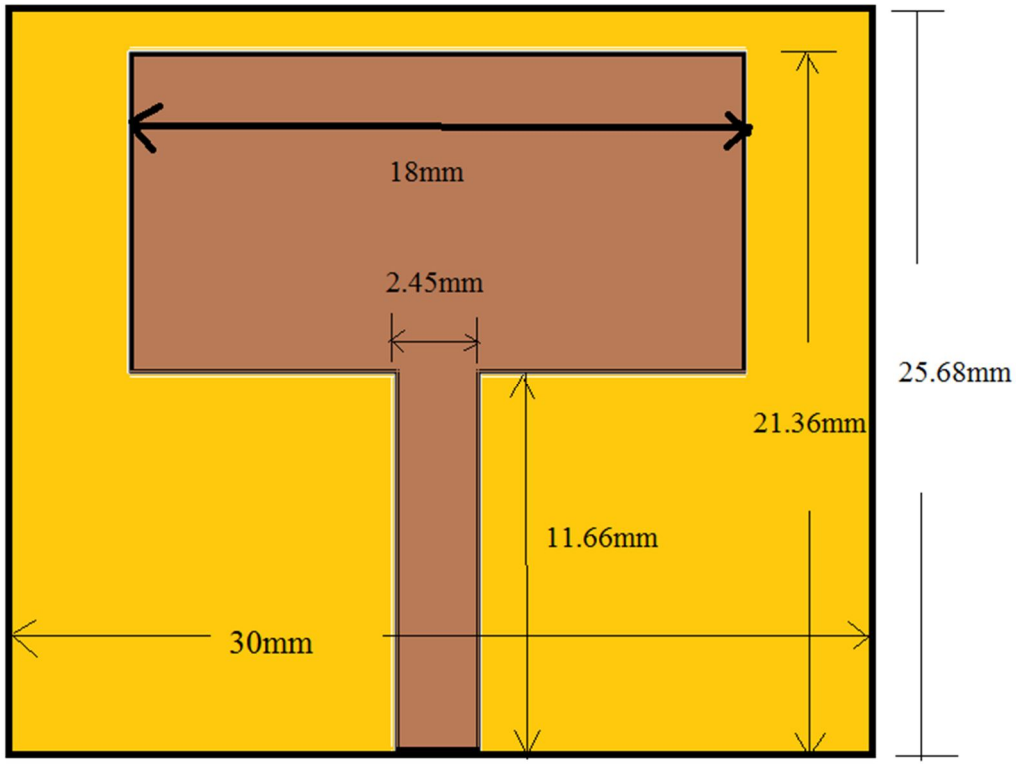

Figure 5.14: Geometry of the patch antenna corresponding to a resonant frequency of 9.4 GHz.

The radiation pattern of this patch antenna is given in Figure 5.15.

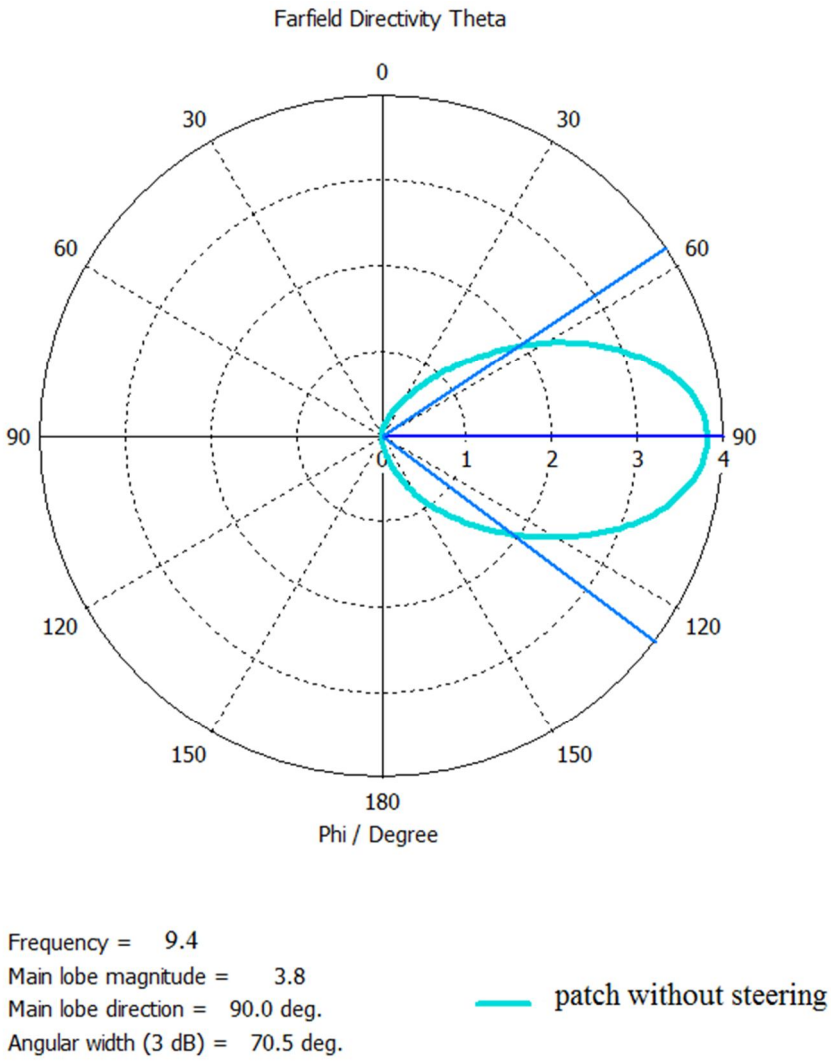

Figure 5.15: Radiation pattern of patch antenna without beam steering

This is the radiation pattern of the antenna without beam steering which is simulated through CST Microwave studio.

5.6 PATCH ANTENNA WITH BEAM STEERING

By varying the phase of the electromagnetic wave radiated by the patch antenna having resonant frequency 9.4 GHz, its beam can be steered in different angles. To achieve this, the varying refractive index omega (Ω) pattern is kept as superstrate to this patch antenna. A four layer metamaterial slab (shown in Figure 5.16 and 5.17) are stacked parallely along x direction.

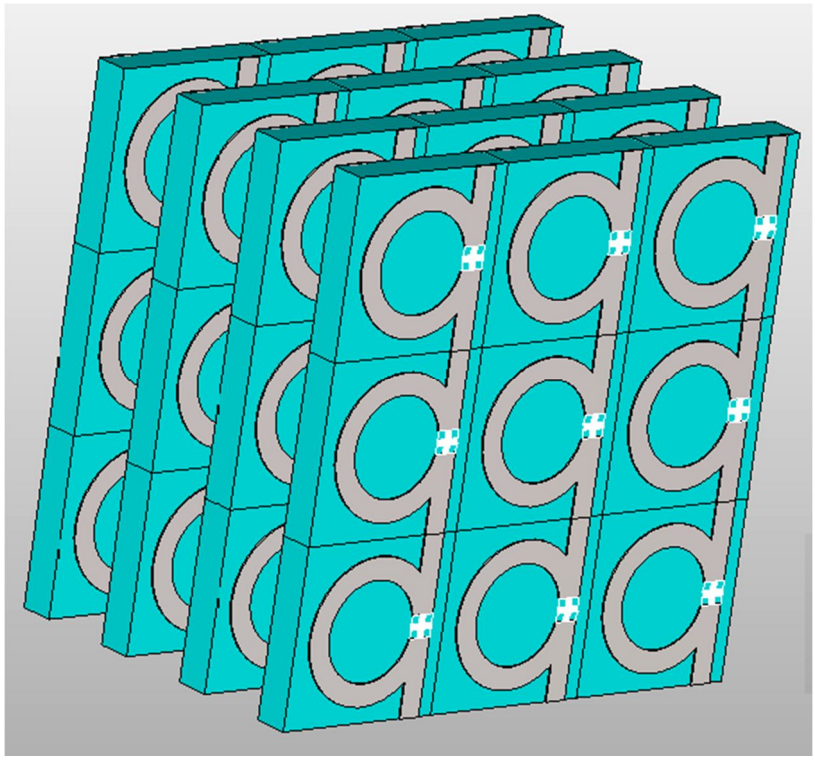

Figure 5.16: A four layer of omega pattern metamaterial slabs

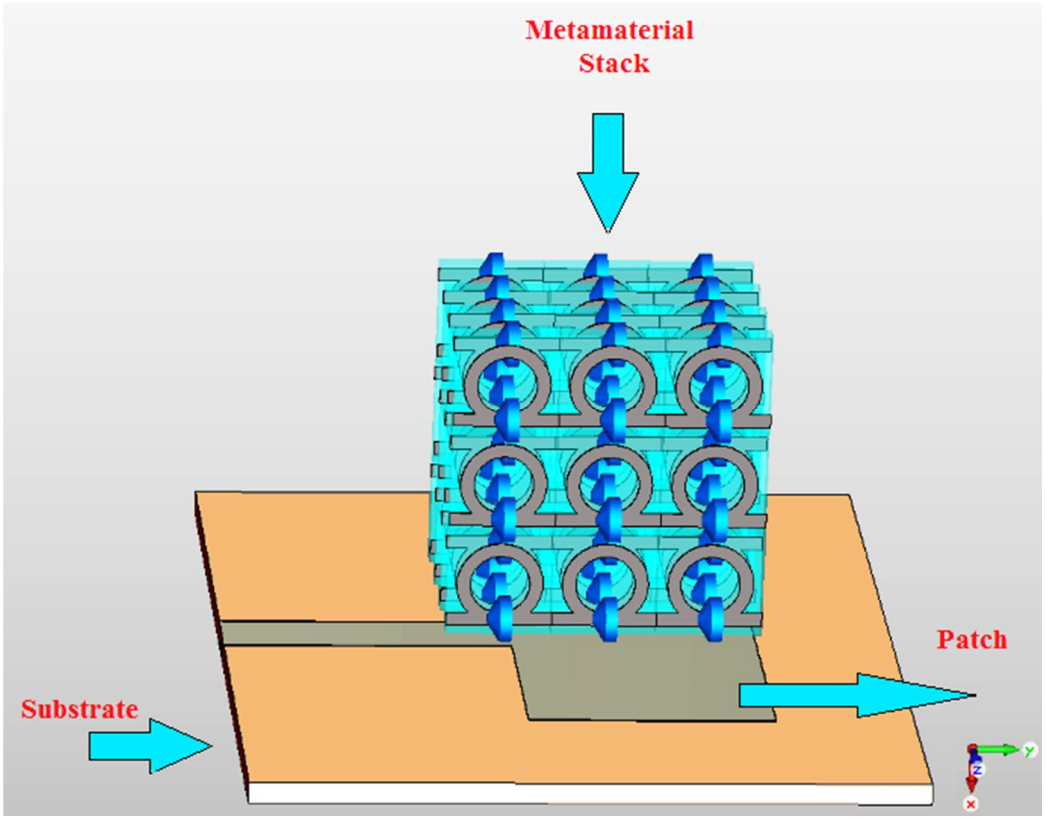

Figure 5.17: 9.4 GHz resonating patch with metamaterial for steering the beam

When the wave passes through this metamaterial structure with varying capacitance connected in between the gap of the omega pattern, its phase undergoes different shifts due to varying refractive index, which results in changing the direction of main lobe. The table below shows the variation of direction of main lobe as capacitance varies.

Variable capacitance (C)	Plasma frequency (ω_p)	Refractive index at 9.4 GHz	Direction of main lobe in degree
0.3 pF	10.61 GHz	-6.134	134^0
0.8 pF	9.75 GHz	-3.252	111^0
1.6 pF	9.11 GHz	1.962	85^0

Table 5.4: Variation of main lobe direction with variable capacitance

The radiation pattern of the patch antenna corresponding to this varying capacitance is shown in Figure 5.18 to 5.21.

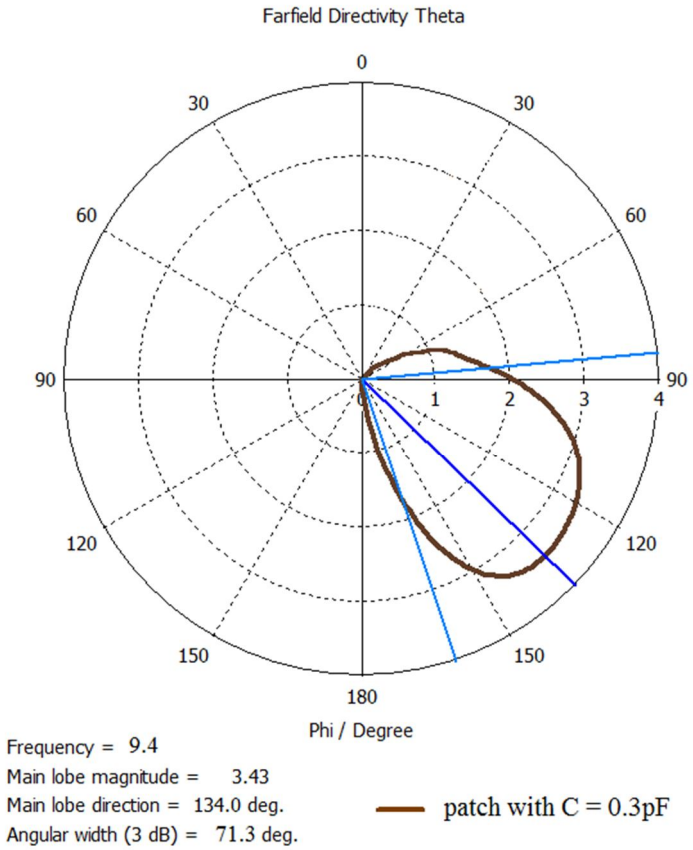

Figure 5.18: Radiation pattern of the antenna with C=0.3 pF

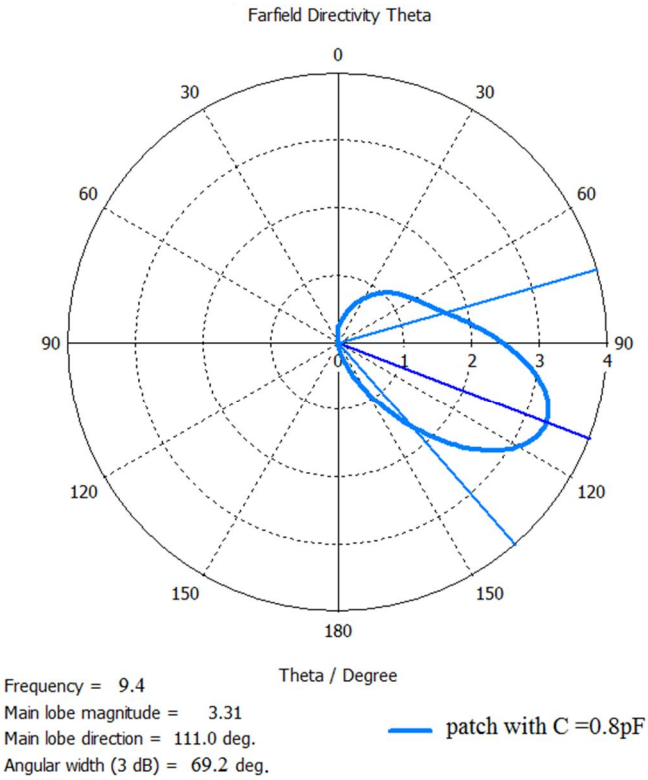

Figure 5.19: Radiation pattern of the antenna with C=0.8 pF

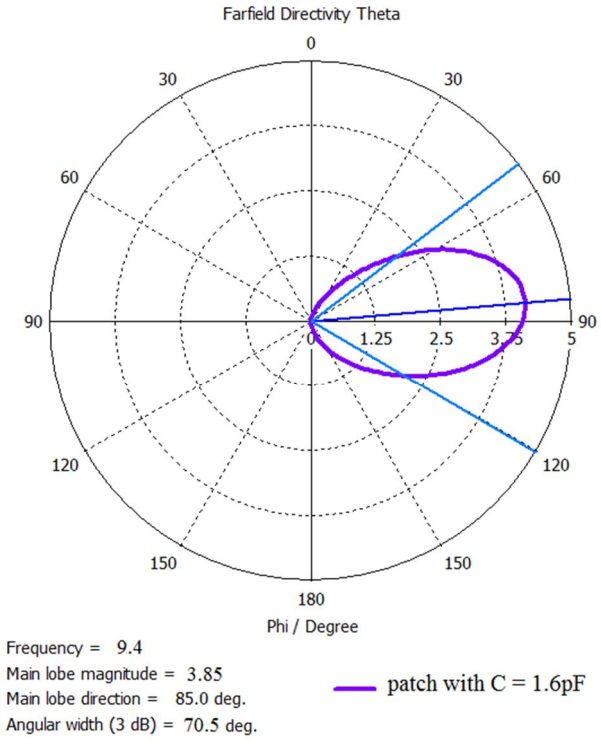

Figure 5.20: Radiation pattern of the antenna with C=1.6 pF

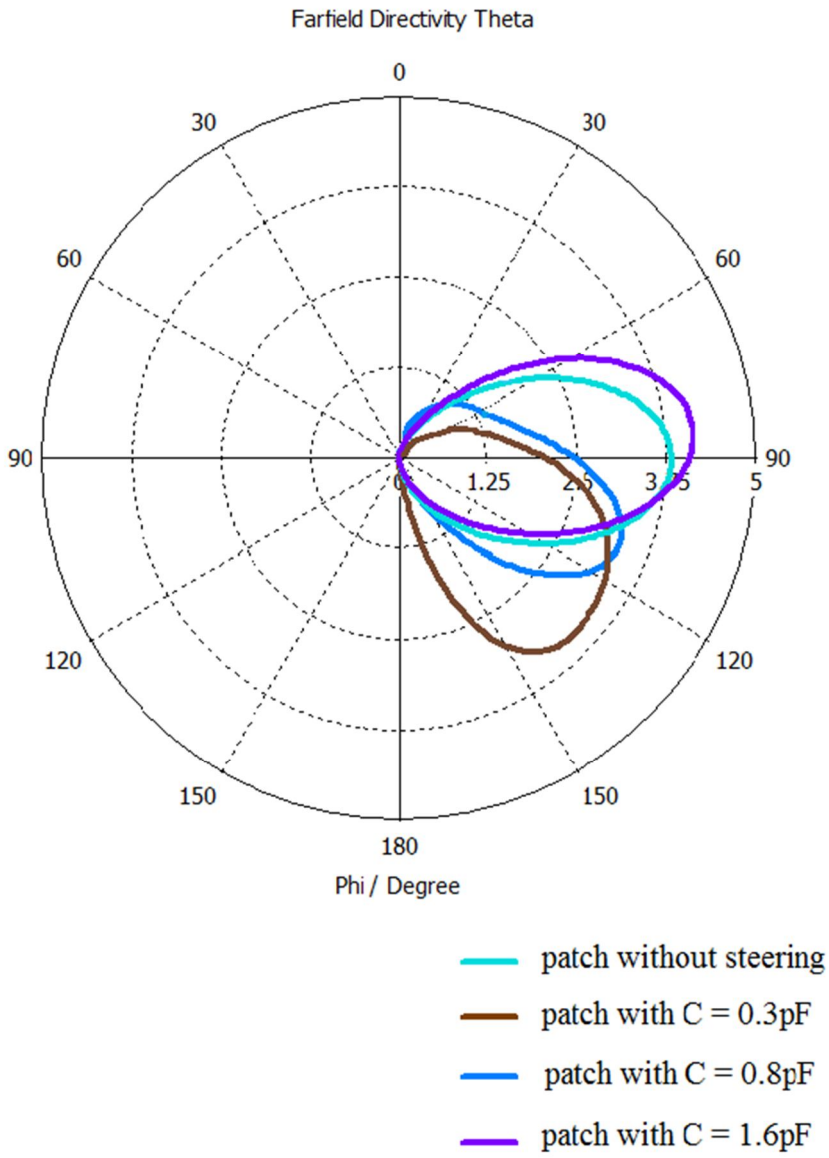

Figure 5.21: Radiation pattern of the antenna with and without steering

From the radiation pattern diagram it can be seen that, when there is no metamaterial superstrate the direction of main lobe of the patch antenna is along 90^0. When the capacitance increases the main lobe shifts towards anticlockwise direction and when the capacitance decreases, the main lobe shifts towards clockwise direction. In this arrangement the beam is steered from 85^0 to 134^0. Hence, the back to back omega pattern can be used for beam steering of an electromagnetic wave.

CHAPTER 6

SUMMARY AND CONCLUSION

- This thesis reports a metamaterial structure showing zero refractive index at 10.255 GHz for constant spatial distribution of electric field.

- A microstrip patch antenna was designed for the same above frequency.

- The 10.255 GHz resonating metamaterial was kept as superstrate to the microstrip antenna, which resulted in improvement in the directivity of the patch antenna. This improvement of directivity resulted due to narrowing of the beam width of the wave coming out of the zero-index metamaterial.

- The simulated structure is experimentally verified for its S parameter, which showed a close agreement to each other.

- This thesis also reports the realization of a back to back connected omega pattern for steering the beam of a patch antenna designed at 9.4 GHz. The advantage of this pattern is that, its cost and complexity is far less compared to the phased array systems currently being used for beam steering purpose. Also the size of the structure is small enough compared to the huge arrangement usually being used to achieve beam shifting.

REFERENCES

1. V. G. Veselago, " The Electrodynamics of Substances with Simultaneously Negative Values of F. and μ", Soy. Phys. Usp, Vol. 10, No: 4, pp. 509-514, 1968.

2. J. B. Pendry, A. J. Holden, D. J. Robbins, and W. J. Stewart, " Magnetism from Conductors and Enhanced Nonlinear Phenomena", IEEE Trans. Microwave Theory Tech., Vol. 47, No: 11, pp. 2075-2084, 1999.

3. Enoch, S.G. Tayeb, P. Sabouroux, and P. Vincont, "A metamaterial for directive emission", Phys. Rev. Lett., Vol. 89, 213902: 1–4, 2002.

4. Pendry, J. B., A. J. Holden, W. J. Stewart, and I. Youngs, "Extremely low frequency plasmons in metallic mesostructures", Phys. Rev. Lett., Vol. 76, No: 25, 4773–4776, 1996.

5. Pendry, J. B., A. J. Holden, D. J. Robbins, and W. J. Stewart, "Low frequency plasmons in thin wire structures", J. Phys.: Condensed Matter., Vol. 10, 4785–4809, 1998.

6. Dong Hyun Lee and Wee Sang, "Extraction of effective permittivity and permeability of periodic metamaterial cells", Park Division of Electronic and Computer Engineering, Pohang University of Science and Technology, San 31, Hyojadong, Namgu, Pohang, Kyungbuk, Korea.

7. Wentworth M. Stuart (2005), "Fundamentals of Electromagnetics with Engineering Applications", pp 442-445, John Wiley & Sons, NJ, USA.

8. Constantine A. Balanis – "Antenna Theory - Analysis and Design" - Third Edition.

9. Wenshan Cai, "Metal-Coated Waveguide Stretches Wavelengths to Infinity", School of Electrical and Computer Engineering, and School of Materials Science and Engineering, Georgia Institute of Technology, Atlanta, GA 30332, USA.

10. Yusuf, Y., Univ. of Central Florida, Orlando, Xun Gong, “ A Low-Cost Patch Antenna Phased Array With Analog Beam Steering Using Mutual Coupling and Reactive Loading”, - IEEE Antennas and wireless propagation letters, Vol. 7, 2008.